Applications of Mathematics

Theofanis Strouboulis; Delin Wang

Guaranteed a-posteriori error estimation for finite element solutions of nonstationary heat conduction problems based on their elliptic reconstructions

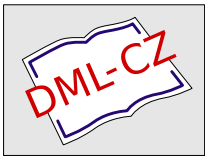
Applications of Mathematics, Vol. 69 (2024), No. 5, 589–619

Persistent URL: http://dml.cz/dmlcz/152632

Terms of use:

© Institute of Mathematics CAS, 2024

Institute of Mathematics of the Czech Academy of Sciences provides access to digitized documents strictly for personal use. Each copy of any part of this document must contain these *Terms of use*.



This document has been digitized, optimized for electronic delivery and stamped with digital signature within the project *DML-CZ: The Czech Digital Mathematics Library* http://dml.cz

69 (2024) APPLICATIONS OF MATHEMATICS No. 5, 589–619

GUARANTEED A-POSTERIORI ERROR ESTIMATION FOR FINITE ELEMENT SOLUTIONS OF NONSTATIONARY HEAT CONDUCTION PROBLEMS BASED ON THEIR ELLIPTIC RECONSTRUCTIONS

Theofanis Strouboulis, Delin Wang, College Station

Received April 9, 2024. Published online September 17, 2024.

Abstract. We deal with the a-posteriori estimation of the error for finite element solutions of nonstationary heat conduction problems with mixed boundary conditions on bounded polygonal domains. The a-posteriori error estimates are constucted by solving stationary "reconstruction" problems, obtained by replacing the time derivative of the exact solution by the time derivative of the finite element solution. The main result is that the reconstructed solutions, or reconstructions, are superconvergent approximations of the exact solution (they are more accurate than the finite element solution) when the error is measured in the gradient or the energy-norm. Because of this, the error in the gradient of the finite element solution can be estimated reliably, by computing its difference from the gradient of its reconstructions. Numerical examples show that "reconstruction estimates" are reliable for the most general classes of solutions which can occur in practical computations.

Keywords: error estimation; elliptic reconstruction; superconvergence

MSC 2020: 65N30

1. Introduction

This paper addresses the a-posteriori estimation of the error in finite element solutions of nonstationary heat conduction problems. The estimates are computed in terms of solutions of steady state problems obtained from the nonstationary problem, by moving the time derivative term of the exact solution to the right-hand side, and by replacing it by the time derivative of the finite element solution. The solutions of these problems are referred to as reconstructions of the finite element solution.

DOI: 10.21136/AM.2024.0085-24

© Institute of Mathematics, Czech Academy of Sciences 2024.

They have much smaller error than the finite element solution, and hence they can be employed to estimate its error. Numerical computations indicate that the error estimates are robust.

In previous works (see [6] and the references therein) the authors researched the a-posteriori estimation for semidiscrete finite element solutions of nonstationary heat conduction problems. The error estimates were constructed by employing solutions of steady state problems obtained from the nonstationary problem by replacing the time derivative of the exact solution by the time derivative of the semidiscrete finite element solution. The reconstruction approach, can be understood as an extension of the idea of "superconvergent recovery" to the nonstationary heat-conduction problem.

In this work the reconstructions are employed for estimating the error in fully discrete finite element solutions, obtained by forward in time integration of the system of semidiscrete finite element ODEs. The error is measured in space-time norms resulting naturally from the space-time inner products, and the exact reconstruction estimates are upper bounds of the error measured in the space-time norms. By "exact" it is meant that the reconstruction problems are solved with negligible error. The fully-discrete finite element solutions include a time-error due to the time-stepping, and require a "temporal reconstruction estimator" for estimating it. Numerical examples illustrate the superconvergence of the reconstructed solutions and the quality of the estimates.

When the error is measured using the L^2-norm, for analytic exact solutions the reconstructions are superconvergent only for elements of quadratic degree or higher; while for exact solutions with algebraic point singulaties there is no supeconvergence for elements of any degree. When the error is measured in the energy norm (the L^2-norm of the gradient), superconvergence also occurs for the most general solutions, which can have many point singularities, and for finite elements of any degree. Computational results show that the reconstruction error estimates are sharp.

2. Nonstationary heat conduction, finite element solutions, and their superconvergent reconstructions

Let Ω be a bounded two-dimensional polygonal domain, which consists of several material subdomains, Ω_i, $i = 1, \ldots, \text{nsubd}$, with boundary $\partial\Omega$ consisting of the Dirichlet part Γ_D, and the Neumann part Γ_N, namely, $\partial\Omega = \Gamma_D \cup \Gamma_N$, and $\Gamma_{ij} \stackrel{\text{def}}{=} \partial\Omega_i \cap \partial\Omega_j$, the intersection of $\partial\Omega_i$, and $\partial\Omega_j$, which could be empty. Let $Q_T \stackrel{\text{def}}{=} \Omega \times (0, T)$ denote the space-time domain for $T > 0$. We will be interested in solving the nonstationary heat conduction problem in orthotropic continua Ω formulated as:

Find $u = u(\mathbf{x}, t)$ such that

$$\gamma_i \frac{\partial u}{\partial t} - \nabla \cdot (\mathbf{K}_i \nabla u) = f \quad \text{in } Q_T^i \stackrel{\text{def}}{=} \Omega_i \times (0,T), \quad i = 1, \ldots, \text{nsubd}, \tag{2.1a}$$

$$u = 0 \quad \text{on } \Gamma_D \times (0,T), \tag{2.1b}$$

$$\mathbf{K}_i(s) \nabla u \cdot \mathbf{n} = g - \alpha(s) u \quad \text{on } (\Gamma_N \cap \partial\Omega_i) \times (0,T), \tag{2.1c}$$

$$u(\cdot, 0) = 0 \quad \text{in } \Omega, \tag{2.1d}$$

where $\mathbf{n}$ is the exterior unit normal. For the conditions of regularity, continuity, integrability, and the admissible spaces for the input data, the reader is referred to [7] and the references therein. These conditions are met in problems of heat conduction in multi material polygonal domains in two space dimensions, which are addressed in this paper.

According to [7], there exists a solution u of (2.1), which satisfies the variational equation

$$\Big(\gamma \frac{\partial u}{\partial t}, v\Big)_{L^2(\Omega)} + \mathscr{B}_\Omega(u, v) = \mathscr{L}(v) \quad \forall\, v \in \mathscr{U}(\Omega), \quad \forall\, t \in (0,T), \tag{2.2}$$

where $\mathscr{U}(\Omega)$ is the energy-space, namely,

$$\mathscr{U}(\Omega) \stackrel{\text{def}}{=} \Big\{ u \,|\, \|u\|_{\mathscr{U}} \stackrel{\text{def}}{=} \sqrt{\int_\Omega |\mathbf{K}\nabla u|^2 + \int_{\Gamma_N} \alpha u^2} < \infty,\ u|_{\Gamma_D} = 0 \Big\}, \tag{2.3a}$$

where

$$\mathscr{B}_\Omega(u, v) \stackrel{\text{def}}{=} \int_\Omega \nabla v^\top \mathbf{K}(x,y) \nabla u + \int_{\Gamma_N} \alpha(s) u v, \quad \mathscr{L}(v) \stackrel{\text{def}}{=} \int_\Omega f v + \int_{\Gamma_N} g v \tag{2.3b}$$

and

$$\Big(\gamma \frac{\partial u}{\partial t}, v\Big)_{L^2(\Omega)} \stackrel{\text{def}}{=} \sum_{i=1}^{\text{nsubd}} \int_{\Omega_i} \gamma_i \frac{\partial u}{\partial t} v. \tag{2.3c}$$

The semidiscrete finite element solution is defined as the solution of the following problem:

Find $u_{S^p_{\Delta_h}} \in S^p_{\Delta_h}$ such that

$$\Big(\gamma \frac{\partial}{\partial t} u_{S^p_{\Delta_h}}, v\Big)_{L^2(\Omega)} + \mathscr{B}_\Omega(u_{S^p_{\Delta_h}}, v) = \mathscr{L}(v) \quad \forall\, v \in S^p_{\Delta_h}, \quad \forall\, t \in (0,T), \tag{2.4}$$

where $S^p_{\Delta_h} \subset \mathscr{U}(\Omega)$ is the finite element space defined using tensor-product rectangular elements of degree p over mesh Δ_h.

The reconstructed solution $\widehat{u}$ in the semidiscrete case [3] is defined as the solution of the following steady state problems:

Find $\widehat{u} \in \mathscr{U}(\Omega)$ such that

$$\mathscr{R}_\Omega(\widehat{u}, v) = \mathscr{L}(v) - \Big(\gamma \frac{\partial}{\partial t} u_{s^p_{\Delta_h}}, v\Big)_{L^2(\Omega)} \quad \forall\, v \in \mathscr{U}(\Omega),\ \forall\, t \in (0,T). \tag{2.5}$$

It follows that

$$\mathscr{B}_\Omega(\widehat{u}, v) = \mathscr{L}(v) - \Big(\gamma \frac{\partial u_{S^p_{\Delta_h}}}{\partial t}, v\Big)_{L^2(\Omega)} = \mathscr{B}_\Omega(u_{S^p_{\Delta_h}}, v) \quad \forall\, v \in S^p_{\Delta_h},\ \forall\, t \in (0,T). \tag{2.6}$$

Equation (2.6) proves that $u_{S^p_{\Delta_h}}$ is the finite element approximation of $\widehat{u}$. In [2], [3], $\widehat{u}$ is called a postprocessed solution and in [5] the elliptic reconstruction.

Next, the fully discrete finite element solution is defined. Let $\{I_n\}_{n=1}^N$ be a partition of the time interval $[0,T]$ into N uniform time steps $I_n = (t_{n-1}, t_n]$, $n = 1, \ldots, N$, $0 = t_0 < t_1 \ldots < t_N = T$, and denote by $\Delta t \stackrel{\text{def}}{=} t_n - t_{n-1}$ the time step size.

For $t \in I_n$, the standard backward Euler-Galerkin method for the discretization of problem (2.1) associated with the finite element spaces $S^p_{\Delta_h}$ is defined as follows:

Find $U^n_{S^p_{\Delta_h}} \in S^p_{\Delta_h}$ such that

$$\gamma\Big(\frac{U^n_{s^p_{\Delta_h}} - U^{n-1}_{s^p_{\Delta_h}}}{\Delta t}, v\Big)_{L^2(\Omega)} + \mathscr{B}_\Omega(U^n_{s^p_{\Delta_h}}, v) = \mathscr{L}^n(v) \quad \forall\, v \in S^p_{\Delta_h},\ \forall\, t \in (t_{n-1}, t_n], \tag{2.7}$$

where

$$\mathscr{L}^n(v) \stackrel{\text{def}}{=} \int_\Omega f^n v + \int_{\Gamma_N} g^n v. \tag{2.8}$$

Here the notations are:

$$U^n_{s^p_{\Delta_h}} \stackrel{\text{def}}{=} U^n_{s^p_{\Delta_h}}(\mathbf{x}, t_n), \quad U^{n-1}_{s^p_{\Delta_h}} \stackrel{\text{def}}{=} U^{n-1}_{s^p_{\Delta_h}}(\mathbf{x}, t_{n-1}), \quad f^n \stackrel{\text{def}}{=} f(\mathbf{x}, t_n), \quad g^n \stackrel{\text{def}}{=} g(\mathbf{x}, t_n)$$

and $S^p_{\Delta_h} \subset \mathscr{U}(\Omega)$ is the finite element space defined using tensor-product rectangular elements of degree p over mesh Δ_h.

From $U^n_{S^p_{\Delta_h}}$ at time t_n, and $U^{n-1}_{S^p_{\Delta_h}}$ at t_{n-1}, we can build a continuous function of time $U_{S^p_{\Delta_h}} \stackrel{\text{def}}{=} U_{S^p_{\Delta_h}}(\mathbf{x}, t)$ for time interval $[t_{n-1}, t_n]$ by piecewise linear interpolation, e.g.,

$$U_{S^p_{\Delta_h}} \stackrel{\text{def}}{=} l_{n-1}(t) U^{n-1}_{S^p_{\Delta_h}} + l_n(t) U^n_{S^p_{\Delta_h}} \quad \text{for } t \in [t_{n-1}, t_n], \tag{2.9}$$

where

$$l_{n-1}(t) \stackrel{\text{def}}{=} \frac{t_n - t}{\Delta t}, \quad l_n(t) \stackrel{\text{def}}{=} \frac{t - t_{n-1}}{\Delta t}. \tag{2.10}$$

The elliptic reconstruction problems, as formulated in [3], [2], can now be extended to the fully discrete finite element solution as the solution of the following problems:

Find $\widehat{U} = \widehat{U}(\mathbf{x}, t)$ such that

$$\mathscr{B}_\Omega(\widehat{U}, v) = \mathscr{L}(v) - \Big(\gamma \frac{\partial}{\partial t} U_{s^p_{\Delta_h}}, v\Big)_{L^2(\Omega)} \quad \forall\, v \in \mathscr{U}(\Omega),\ \forall\, t \in (0, T). \tag{2.11}$$

The finite element approximation of (2.11) in space $S^p_{\Delta_h}$ is the following:

$$\mathscr{B}_\Omega(\widehat{U}_{S^p_{\Delta_h}}, v) = \mathscr{L}(v) - \Big(\gamma \frac{\partial}{\partial t} U_{S^p_{\Delta_h}}, v\Big)_{L^2(\Omega)} \quad \forall\, v \in S^p_{\Delta_h},\ \forall\, t \in (0, T). \tag{2.12}$$

Note that the finite element solution $\widehat{U}_{S^p_{\Delta_h}}$ of equation (2.11) is equivalent to the fully discrete finite element solution $U_{S^p_{\Delta_h}}$ only at time instant $t = t_n, n = 0, 1, \ldots, N$, namely,

$$\mathscr{B}_\Omega(\widehat{U}^n_{S^p_{\Delta_h}}, v) = \mathscr{L}^n(v) - \Big(\gamma \frac{\partial}{\partial t} U_{S^p_{\Delta_h}}, v\Big)_{L^2(\Omega)} = \mathscr{B}_\Omega(U^n_{S^p_{\Delta_h}}, v) \quad \forall\, v \in S^p_{\Delta_h} \tag{2.13}$$

with

$$\frac{\partial}{\partial t} U_{S^p_{\Delta_h}} = \frac{U^n_{S^p_{\Delta_h}} - U^{n-1}_{S^p_{\Delta_h}}}{\Delta t}. \tag{2.14}$$

Let us define the exact error between the exact solution u and its fully discrete finite element approximation $U_{S^p_{\Delta_h}}$ at any time instant t by

$$E_h \stackrel{\text{def}}{=} u - U_{S^p_{\Delta_h}}, \tag{2.15}$$

then at time instant $t = t_n$, $n = 0, 1, \ldots, N$, we have by the triangle inequality

$$\|E^n_h\|_{H^l} = \|u^n - U^n_{s^p_{\Delta_h}}\|_{H^l} \leqslant \|u^n - \widehat{U}^n\|_{H^l} + \|\widehat{U}^n - U^n_{S^p_{\Delta_h}}\|_{H^l}, \quad l = 0, 1, \tag{2.16}$$

where $\widehat{U}^n$ is the exact solution of equation (2.11) at time instant t_n.

Because $U^n_{S^p_{\Delta_h}}$ is the finite element approximation of $\widehat{U}^n$ based on finite element space $S^p_{\Delta_h}$, we know that $\|\widehat{U}^n - U^n_{S^p_{\Delta_h}}\|_{H^l}$ is the spatial error term with the following bounds for sufficiently smooth solution:

$$\|\widehat{U}^n - U^n_{S^p_{\Delta_h}}\|_{H^l} \leqslant C h^{p+1-l}, \quad l = 0, 1. \tag{2.17}$$

By introducing the exact solution $\widehat{u}^n$ of equation (2.5) at time instant t_n, we can split $u^n - \widehat{U}^n$ the following way,

$$u^n - \widehat{U}^n = u^n - \widehat{u}^n + \widehat{u}^n - \widehat{U}^n. \tag{2.18}$$

From the triangle inequality it follows that

$$\|u^n - \widehat{U}^n\|_{H^l} \leqslant \|u^n - \widehat{u}^n\|_{H^l} + \|\widehat{u}^n - \widehat{U}^n\|_{H^l}, \quad l = 0, 1. \tag{2.19}$$

Clearly $\|u^n - \widehat{u}^n\|_{H^l}$ is the spatial error term and its convergence rate is well defined by the theorem proven in [6], while $\|\widehat{u}^n - \widehat{U}^n\|_{H^l}$ is the temporal error. For quasi-uniform meshes and uniform time step size Δt, for the backward difference scheme we have the following bounds [1]:

$$\|\widehat{u}^n - \widehat{U}^n\|_{H^l} \leqslant C\Delta t, \quad l = 0, 1. \tag{2.20}$$

Therefore, we have

$$\|E_h^n\|_{H^l} \leqslant C(h^{p+1-l} + h^{p+2-l}|\log h| + \Delta t), \quad p > 1,\ l = 0, 1, \tag{2.21a}$$

$$\|E_h^n\|_{H^l} \leqslant C(h^{2-l} + h^2|\log h|^l + \Delta t), \quad p = 1,\ l = 0, 1. \tag{2.21b}$$

It follows that if the temporal error term $\|\widehat{u}^n - \widehat{U}^n\|_{H^l}$ is negligible, and the term $\|u^n - \widehat{u}^n\|_{H^l}$ is superconvergent, we have

$$\|E_h^n\|_{H^l} \approx \|\widehat{U}^n - U^n_{S^p_{\Delta_h}}\|_{H^l}, \quad l = 0, 1. \tag{2.22}$$

3. Upper bound in space-time norm

Theorem 3.1. *The error E_h measured in the $\mathscr{C}$-norm,*

$$\|v\|_{\mathscr{C}} \stackrel{\text{def}}{=} \sqrt{\int_0^T (T-t)\|v\|^2_{\mathscr{U}}\,\mathrm{d}t + \int_0^T \|\sqrt{\gamma}v\|^2_{L^2}\,\mathrm{d}t}, \tag{3.1a}$$

has the upper bound

(3.1b)

$$\|E_h\|_{\mathscr{C}} \leqslant \mathscr{F}^{\mathrm{FD}}_{EX} \stackrel{\text{def}}{=} \sqrt{\int_0^T (T-t)(\|\widehat{U} - \widehat{U}_{S^p_{\Delta_h}}\|^2_{\mathscr{U}} + \|\widehat{U}_{S^p_{\Delta_h}} - U_{S^p_{\Delta_h}}\|^2_{\mathscr{U}})\,\mathrm{d}t + T\|\sqrt{\gamma}E_h(0)\|^2_{L^2}},$$

where $E_h(0)$ denotes the exact error at time instant $t = 0$.

P r o o f. Substracting equation (2.11) from equation (2.2), we have

$$\Big(\gamma\frac{\partial}{\partial t}E_h, v\Big)_{L^2(\Omega)} + \mathscr{B}_\Omega(u - \widehat{U}, v) = 0 \quad \forall\, v \in \mathscr{U}(\Omega),\ \forall\, t \in (0, T). \tag{3.2}$$

Letting $v = E_h$, we obtain

$$\frac{1}{2}\frac{\mathrm{d}}{\mathrm{d}t}\|\sqrt{\gamma}E_h\|^2_{L^2} + \mathscr{B}_\Omega(u - \widehat{U}, E_h) = 0 \quad \forall\, t \in (0, T). \tag{3.3}$$

It can be shown that

$$\mathscr{B}_\Omega(u-\widehat{U},E_h)=\|u-\widehat{U}\|^2_{\mathscr{U}}-\|\widehat{U}-U_{s^p_{\Delta_h}}\|^2_{\mathscr{U}}+\|E_h\|^2_{\mathscr{U}}-\mathscr{B}_\Omega(E_h,u-\widehat{U}), \tag{3.4}$$

from which it follows that

$$\mathscr{B}_\Omega(u-\widehat{U},E_h)=\frac{1}{2}(\|E_h\|^2_{\mathscr{U}}+\|u-\widehat{U}\|^2_{\mathscr{U}}-\|\widehat{U}-U_{S^p_{\Delta_h}}\|^2_{\mathscr{U}}). \tag{3.5}$$

Therefore, we have

$$\frac{\mathrm{d}}{\mathrm{d}t}\|\sqrt{\gamma}E_h\|^2_{L^2}+\|E_h\|^2_{\mathscr{U}}+\|u-\widehat{U}\|^2_{\mathscr{U}}=\|\widehat{U}-U_{S^p_{\Delta_h}}\|^2_{\mathscr{U}}. \tag{3.6}$$

Noting that $\widehat{U}_{S^p_{\Delta_h}}$ is the finite element approximation of (2.11) in $S^p_{\Delta_h}$, we have the orthogonality

$$\mathscr{B}_\Omega(\widehat{U}-\widehat{U}_{S^p_{\Delta_h}},\widehat{U}_{S^p_{\Delta_h}}-U_{S^p_{\Delta_h}})=0, \tag{3.7}$$

from which it follows that

$$\|\widehat{U}-U_{S^p_{\Delta_h}}\|^2_{\mathscr{U}}=\|\widehat{U}-\widehat{U}_{S^p_{\Delta_h}}\|^2_{\mathscr{U}}+\|\widehat{U}_{S^p_{\Delta_h}}-U_{S^p_{\Delta_h}}\|^2_{\mathscr{U}}. \tag{3.8}$$

Integrating twice $\int_0^T\int_0^\tau$, on both sides of (3.6) and employing Fubini's theorem, we obtain

$$\begin{aligned}\int_0^T(\|\sqrt{\gamma}E_h\|^2_{L^2}+(T-t)\|E_h\|^2_{\mathscr{U}})\,\mathrm{d}t+\int_0^T(T-t)\|u-\widehat{U}\|^2_{\mathscr{U}}\,\mathrm{d}t\\ =\int_0^T(T-t)(\|\widehat{U}-\widehat{U}_{S^p_{\Delta_h}}\|^2_{\mathscr{U}}+\|\widehat{U}_{S^p_{\Delta_h}}-U_{S^p_{\Delta_h}}\|^2_{\mathscr{U}})\,\mathrm{d}t+T\|\sqrt{\gamma}E_h(0)\|^2_{L^2}.\end{aligned} \tag{3.9}$$

By dropping the term $\|u-\widehat{U}\|^2_{\mathscr{U}}$, (3.9) immediately yields (3.1). □

Remark 3.1. If

$$\int_0^T(T-t)\|u-\widehat{U}\|^2_{\mathscr{U}}\,\mathrm{d}t<<\int_0^T(\|\sqrt{\gamma}E_h\|^2_{L^2}+(T-t)\|E_h\|^2_{\mathscr{U}})\,\mathrm{d}t,$$

the upper bound $\mathcal{E}_{EX}$ is sharp.

With the introduction of $\mathscr{F}^{\mathrm{FD}}_{EX}$, we can define effectivity index to measure the error E_h of the fully discrete finite element solution $U_{S^p_{\Delta_h}}$ as shown below:

$$\kappa^{\mathrm{FD}}\overset{\mathrm{def}}{=}\frac{\mathscr{F}^{\mathrm{FD}}_{EX}}{\|E_h\|_{\mathscr{E}}}. \tag{3.10}$$

In practice, the exact solution $\widehat{U}$ of the elliptic reconstruction problem (2.11) is not computable and thus the upper bound $\mathscr{F}_{EX}^{\mathrm{FD}}$ is unknown. However, $\widehat{U}$ can be approximated by the nested refinement of the finite element mesh for $U_{S^p_{\Delta_h}}$ (h method) or the increase of polynomial order (p method), or both (hp method).

Let $\widehat{U}_{S_{\Delta_{h'}^{p+k}}}$ be the approximation of the exact solution $\widehat{U}$, where $p+k$ denotes the polynomial space of degree $p+k$ and the mesh $\Delta_{h'}$ is obtained from the uniform nested subdivision of the mesh Δ_h employed to obtain the fully discrete finite element solution $U_{S^p_{\Delta_h}}$. Then, we can define the following computable version of upper bound $\mathscr{F}_{EX}^{\mathrm{FD}}$:

$$\mathscr{F}^{\mathrm{FD}}_{S^{p+k}_{\Delta_{h'}}} \stackrel{\mathrm{def}}{=} \sqrt{\int_0^T (T-t)\|\widehat{U}_{S^{p+k}_{\Delta_{h'}}} - U_{S^p_{\Delta_h}}\|^2_{\mathscr{U}}\,\mathrm{d}t + T\|\sqrt{\gamma}E_h(0)\|^2_{L^2}}. \tag{3.11}$$

It should be noted that $\mathscr{F}^{\mathrm{FD}}_{S^{p+k}_{\Delta_{h'}}}$ is not necessary a guaranteed upper bound.

Let us define the effectivity index of the $\mathscr{F}^{\mathrm{FD}}_{S^{p+k}_{\Delta_{h'}}}$ by

$$\kappa^{\mathrm{FD}}_{S^{\mathrm{FD}}_{\Delta_{h'}}} \stackrel{\mathrm{def}}{=} \frac{\mathscr{F}^{\mathrm{FD}}_{S^{p+k}_{\Delta_{h'}}}}{\|E_h\|_{\mathscr{E}}}. \tag{3.12}$$

We will split the error E_h into two parts

$$E_h = \varrho_h + \theta_h, \tag{3.13}$$

where ϱ_h is the spatial error

$$\varrho_h \stackrel{\mathrm{def}}{=} u - u_{S^p_{\Delta_h}}. \tag{3.14}$$

and θ_h is the temporal error

$$\theta_h \stackrel{\mathrm{def}}{=} u_{S^p_{\Delta_h}} - U_{S^p_{\Delta_h}}. \tag{3.15}$$

We will denote the ratio of the spatial error to the total error by

$$\alpha \stackrel{\mathrm{def}}{=} \frac{\|\varrho_h\|_{\mathscr{E}}}{\|E_h\|_{\mathscr{E}}} \times 100\% \tag{3.16}$$

and the ratio of the temporal error to the total error by

$$\beta \stackrel{\mathrm{def}}{=} \frac{\|\theta_h\|_{\mathscr{E}}}{\|E_h\|_{\mathscr{E}}} \times 100\%. \tag{3.17}$$

Theorem 3.2. *The temporal error θ_h measured in spacetime $\mathscr{C}$-norm has the following upper bound:*

$$\|\theta_h\|_{\mathscr{C}} \leqslant \mathscr{T}^{\mathrm{FD}}_{S^p_{\Delta_h}} \stackrel{\mathrm{def}}{=} \sqrt{\int_0^T (T-t)\|\widehat{U}_{S^p_{\Delta_h}} - U_{S^p_{\Delta_h}}\|^2_{\mathscr{U}}\,\mathrm{d}t}. \tag{3.18}$$

P r o o f. Substracting equation (2.12) from equation (2.4), we have

$$\Big(\gamma\frac{\partial}{\partial t}\theta_h, v\Big)_{L^2(\Omega)} + \mathscr{B}_\Omega(u_{S^p_{\Delta_h}} - \widehat{U}_{S^p_{\Delta_h}}, v) = 0 \quad \forall\, v \in S^p_{\Delta_h},\ \forall\, t \in (0,T). \tag{3.19}$$

Letting $v = \theta_h$, we obtain

$$\frac{1}{2}\frac{\mathrm{d}}{\mathrm{d}t}\|\sqrt{\gamma}\theta_h\|^2_{L^2} + \mathscr{B}_\Omega(u_{S^p_{\Delta_h}} - \widehat{U}_{S^p_{\Delta_h}}, \theta_h) = 0 \quad \forall\, t \in (0,T). \tag{3.20}$$

It can be shown that

$$2\mathscr{B}_\Omega(u_{S^p_{\Delta_h}} - \widehat{U}_{S^p_{\Delta_h}}, \theta_h) = \|u_{S^p_{\Delta_h}} - \widehat{U}_{S^p_{\Delta_h}}\|^2_{\mathscr{U}} - \|\widehat{U}_{S^p_{\Delta_h}} - U_{S^p_{\Delta_h}}\|^2_{\mathscr{U}} + \|\theta_h\|^2_{\mathscr{U}}. \tag{3.21}$$

Therefore, we have

$$\frac{\mathrm{d}}{\mathrm{d}t}\|\sqrt{\gamma}\theta_h\|^2_{L^2} + \|\theta_h\|^2_{\mathscr{U}} + \|u_{S^p_{\Delta_h}} - \widehat{U}_{S^p_{\Delta_h}}\|^2_{\mathscr{U}} = \|\widehat{U}_{S^p_{\Delta_h}} - U_{S^p_{\Delta_h}}\|^2_{\mathscr{U}}. \tag{3.22}$$

Integrating twice, $\int_0^T\int_0^\tau$, both sides of (3.22) and employing Fubini's theorem, we obtain

$$\begin{aligned}\int_0^T (\|\sqrt{\gamma}\theta_h\|^2_{L^2} + (T-t)\|\theta_h\|^2_{\mathscr{U}})\,\mathrm{d}t + \int_0^T (T-t)\|u_{S^p_{\Delta_h}} - \widehat{U}_{S^p_{\Delta_h}}\|^2_{\mathscr{U}}\,\mathrm{d}t \\ = \int_0^T (T-t)\|\widehat{U}_{S^p_{\Delta_h}} - U_{S^p_{\Delta_h}}\|^2_{\mathscr{U}}\,\mathrm{d}t.\end{aligned} \tag{3.23}$$

Note that the temporal error at time instant $t = 0$ satisfies $\theta_h(0) = 0$. Dropping the term

$$\int_0^T (T-t)\|u_{S^p_{\Delta_h}} - \widehat{U}_{S^p_{\Delta_h}}\|^2_{\mathscr{U}}\,\mathrm{d}t,$$

we obtain the upper bound for the temporal error $\|\theta_h\|_{\mathscr{U}(\Omega)}$. □

R e m a r k 3.2. Note that $\mathscr{T}^{\mathrm{FD}}_{S^p_{\Delta_h}} \leqslant \mathscr{F}^{\mathrm{FD}}_{EX}$, since

$$\mathscr{F}^{\mathrm{FD}}_{EX} = \sqrt{\int_0^T (T-t)\|\widehat{U} - \widehat{U}_{S^p_{\Delta_h}}\|^2_{\mathscr{U}}\,\mathrm{d}t + (\mathscr{T}^{\mathrm{FD}}_{S^p_{\Delta_h}})^2 + T\|\sqrt{\gamma}E_h(0)\|^2_{L^2}} \tag{3.24}$$

according to (3.1) and (3.18). And the terms $\|\widehat{U} - \widehat{U}_{S^p_{\Delta_h}}\|_{\mathscr{U}}$ and $\|\sqrt{\gamma}E_h(0)\|^2_{L^2}$ have spatial error only.

R e m a r k 3.3. It should be noted that unlike $\mathscr{F}_{EX}^{\mathrm{FD}}$, which is not computable, here $\mathscr{T}_{S^p_{\Delta_h}}^{\mathrm{FD}}$ is computable and unlike the computable version $\mathscr{F}_{S^{p+k}_{\Delta_{h'}}}^{\mathrm{FD}}$, which might not be a guaranteed upper bound, $\mathscr{T}_{S^p_{\Delta_h}}^{\mathrm{FD}}$ is a guaranteed upper bound for the temporal error.

R e m a r k 3.4. Note that at each time integration point, an elliptic problem of (2.12) has to be solved for $\widehat{U}_{S^p_{\Delta_h}}$. However, the global stiffness matrix of (2.12) only needs to be factorized once and saved on the hard disk for the whole time interval $(0,T]$, and the only computational cost is to form the right-hand-side load vector of (2.12).

Theorem 3.3. *At any time instant, the term* $\|u_{S^p_{\Delta_h}} - \widehat{U}_{S^p_{\Delta_h}}\|^2_{\mathscr{U}}$ *is bounded as follows:*

$$\|u_{S^p_{\Delta_h}} - \widehat{U}_{S^p_{\Delta_h}}\|_{\mathscr{U}} \leqslant \|\widehat{u} - \widehat{U}\|_{\mathscr{U}}. \tag{3.25}$$

P r o o f. Since $u_{S^p_{\Delta_h}} - \widehat{U}_{S^p_{\Delta_h}} \in S^p_{\Delta_h}$, for semi-discrete finite element solution $u_{S^p_{\Delta_h}}$, we have the orthogonality condition

$$\mathscr{B}_\Omega(\widehat{u} - u_{S^p_{\Delta_h}}, u_{S^p_{\Delta_h}} - \widehat{U}_{S^p_{\Delta_h}}) = 0, \tag{3.26}$$

while for fully discrete finite element solution $\widehat{U}_{S^p_{\Delta_h}}$, the orthogonality condition is

$$\mathscr{B}_\Omega(\widehat{U} - \widehat{U}_{S^p_{\Delta_h}}, u_{s^p_{\Delta_h}} - \widehat{U}_{S^p_{\Delta_h}}) = 0. \tag{3.27}$$

Subtracting (3.27) from (3.26), we have

$$\mathscr{B}_\Omega(\widehat{u} - \widehat{U}, u_{S^p_{\Delta_h}} - \widehat{U}_{S^p_{\Delta_h}}) = \|u_{s^p_{\Delta_h}} - \widehat{U}_{S^p_{\Delta_h}}\|^2_{\mathscr{U}}. \tag{3.28}$$

Given the fact

$$\mathscr{B}_\Omega(\widehat{u} - \widehat{U}, u_{S^p_{\Delta_h}} - \widehat{U}_{S^p_{\Delta_h}}) \leqslant \|\widehat{u} - \widehat{U}\|_{\mathscr{U}} \|u_{S^p_{\Delta_h}} - \widehat{U}_{S^p_{\Delta_h}}\|_{\mathscr{U}}, \tag{3.29}$$

we can see (3.25) holds. □

The effectivity index for $\mathscr{T}_{S^p_{\Delta_h}}^{\mathrm{FD}}$, the estimator of the energy-norm of the temporal error θ_h, will be denoted by

$$\zeta_{S^p_{\Delta_h}}^{\mathrm{FD}} \stackrel{\mathrm{def}}{=} \frac{\mathscr{T}_{S^p_{\Delta_h}}^{\mathrm{FD}}}{\|\theta_h\|_{\mathscr{E}}}. \tag{3.30}$$

Note that $\mathscr{T}_{S^p_{\Delta_h}}^{\mathrm{FD}}$ is guaranteed computable upper bound for the temporal error.

The estimator of the norm of the total error $\|E_h\|_{\mathscr{E}}$ is $\mathscr{F}_{EX}^{\mathrm{FD}}$, while the estimator for the norm of the temporal error is $\mathscr{T}_{S^p_{\Delta_h}}^{\mathrm{FD}}$. Therefore, we have the following estimate for the exact temporal error ratio β

$$\beta^{\mathrm{FD}} \stackrel{\mathrm{def}}{=} \frac{\mathscr{T}_{S^p_{\Delta_h}}^{\mathrm{FD}}}{\mathscr{F}_{EX}^{\mathrm{FD}}} \times 100\%. \tag{3.31}$$

If we employ the computable version of $\mathscr{F}_{EX}^{\mathrm{FD}}$, we have

$$\beta_{S^{p+k}_{\Delta_h}}^{\mathrm{FD}} \stackrel{\mathrm{def}}{=} \frac{\mathscr{T}_{S^p_{\Delta_h}}^{\mathrm{FD}}}{\mathscr{F}_{S^{p+k}_{\Delta_h}}^{\mathrm{FD}}} \times 100\%. \tag{3.32}$$

R e m a r k 3.5. If the temporal error $\|\theta_h\|_{\mathscr{E}}$ is dominant in the total error $\|E_h\|_{\mathscr{E}}$, namely, $\|\theta_h\|_{\mathscr{E}} \approx \|E_h\|_{\mathscr{E}}$, we have according to (3.24)

$$\mathscr{F}_{EX}^{\mathrm{FD}} \approx \mathscr{T}_{S^p_{\Delta_h}}^{\mathrm{FD}}, \tag{3.33}$$

and hence,

$$\kappa^{\mathrm{FD}} \approx \zeta_{S^p_{\Delta_h}}^{\mathrm{FD}}. \tag{3.34}$$

4. Numerical examples

E x a m p l e 4.1. Heat transfer problem in one dimension.

Consider the following nonstationary heat conduction problem:

$$\frac{\partial u}{\partial t} - \frac{\partial^2 u}{\partial x^2} = f \quad \text{on } \Omega_T = (0, L) \times (0, T], \tag{4.1a}$$

$$u(x, 0) = 0, \quad 0 < x < L, \tag{4.1b}$$

$$u(0, t) = u(L, t) = 0, \tag{4.1c}$$

with $L = 4$, $T = 4$, and input $f = f(x, t)$ such that the exact solution is given by

$$u(x, t) = \frac{L^2}{\pi^2}(1 - \mathrm{e}^{-\pi^2 t/L^2}) \sin \frac{\pi x}{L}. \tag{4.1d}$$

Figure 1 shows the variation of the relative error versus the time step size for four nested mesh sizes

$$\varepsilon \stackrel{\mathrm{def}}{=} \frac{\|E_h\|_{\mathscr{E}}}{\|u\|_{\mathscr{E}}} \times 100\%, \tag{4.2}$$

while Figure 2 graphs the variation of the ratio of spatial error to the total error α and the ratio of the temporal error to the total error β for the same four nested mesh sizes.

It can be seen that with the increase in mesh refinement level, polynomial order p, the number of time steps, the relative error ε goes down. In the case of $p = 3$, the mesh refinement has no effect on the relative error, which indicates that the temporal error is dominant as shown in Figure 2 for $p = 3$. For linear element $p = 1$, we can see from Figure 2 that with the increase of time steps, the spatial error becomes dominant. As a matter of fact, for coarse mesh, Mesh 1, the spatial error is dominant for all four time step sizes. In the case of cubic element $p = 3$, the spatial error is negligible and temporal error is dominant.

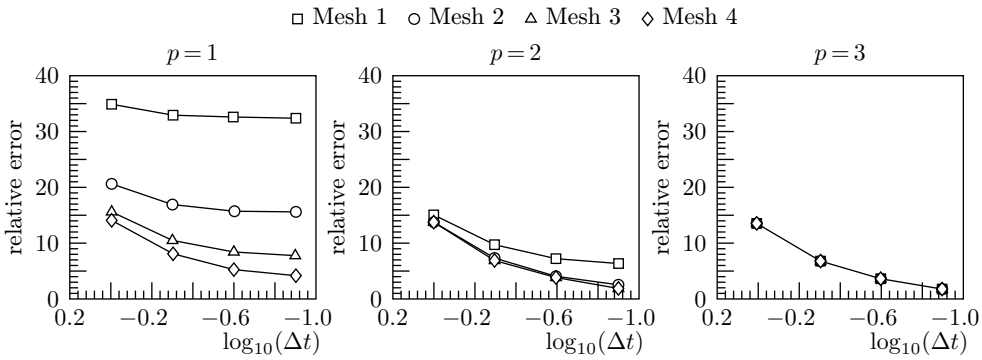


Figure 1. Heat transfer problem in one dimension. The relative error ε for the fully discrete finite element solutions of degree $p = 1, 2$, and 3 computed with four different mesh sizes and four different time step sizes.

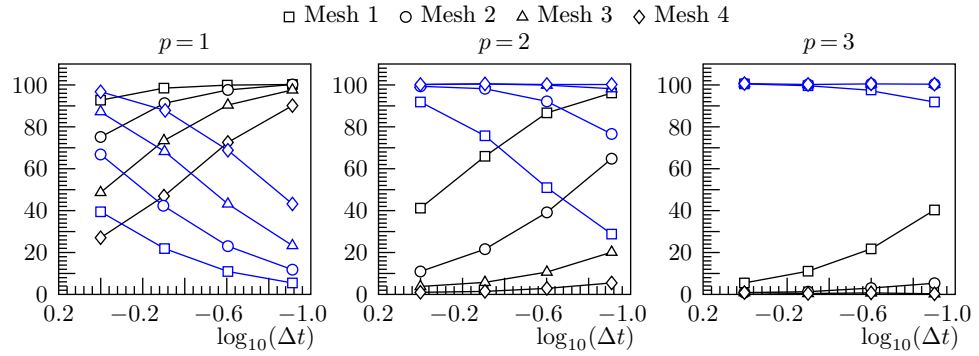


Figure 2. Heat transfer problem in one dimension. The ratio of temporal error β (blue line) and the ratio of spatial error α (black line) for the fully discrete finite element solutions of degree $p = 1, 2$, and 3 computed with four different mesh sizes and four different time step sizes.

Figure 3 graphs the effectivity index κ^{FD} for the total error $\|E_h\|_{\mathscr{E}}$ and the effectivity index $\zeta^{\mathrm{FD}}_{S^p_{\Delta_h}}$ for the temporal error $\|\theta_h\|_{\mathscr{E}}$ for the fully discrete finite element solutions $U_{S^p_{\Delta_h}}$ of degree $p = 1, 2$, and 3. It can be seen that as the spatial error is

made negligible, the effectivity index κ^{FD} converges to the effectivity index $\zeta^{\mathrm{FD}}_{S^p_{\Delta_h}}$ for the temporal error around the value of 1.65 as shown in the case of $p = 3$. Based on Figure 2, we can also see that κ^{FD} is close to 1 as long as the spatial error is dominant.

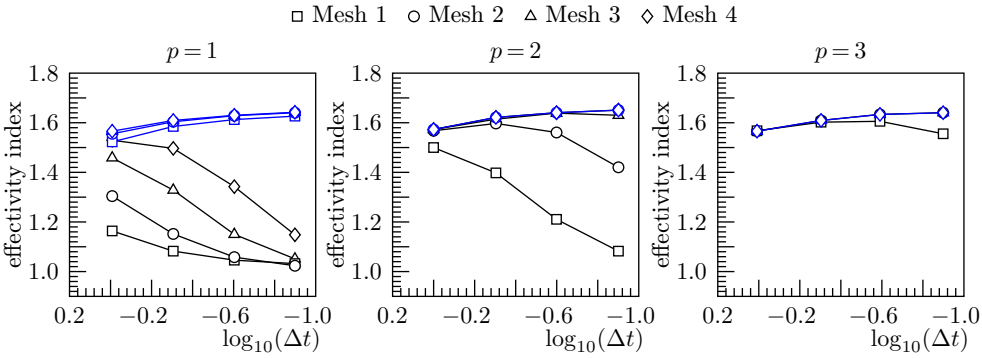


Figure 3. Heat transfer problem in one dimension. The effectivity index κ^{FD} (black line) for the total error $\|E_h\|_{\mathscr{E}}$ and the effectivity index $\zeta^{\mathrm{FD}}_{S^p_{\Delta_h}}$ (blue line) for the temporal error $\|\theta_h\|_{\mathscr{E}}$ for the fully discrete finite element solutions of degree $p = 1, 2$, and 3 computed with four different mesh sizes and four different time step sizes.

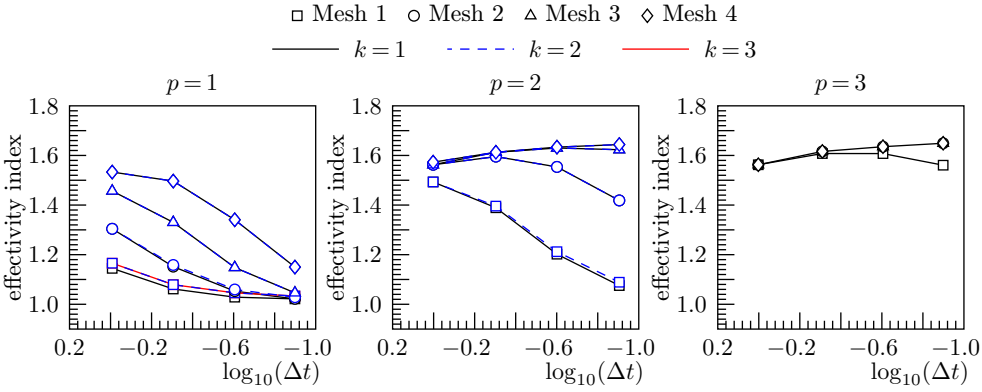


Figure 4. Heat transfer problem in one dimension. The effectivity index $\kappa^{\mathrm{FD}}_{S^p_{\Delta_h}}$ for the total error $\|E_h\|_{\mathscr{E}}$ for the fully discrete finite element solutions of degree $p = 1, 2$, and 3 computed with four different mesh sizes and four different time step sizes.

Figure 4 graphs the effectivity index $\kappa^{\mathrm{FD}}_{S^{p+k}_{\Delta_h}}$ based on the approximation $\widehat{U}_{S^{p+k}_{\Delta_{h'}}}$ of $\widehat{U}$ computed using $p+k, k = 1, 2$, and 3. Here $\Delta_{h'}$ denotes the mesh obtained from the uniform nested subdivision of the mesh Δ_h. In this example we fix the mesh, i.e., $\Delta_{h'} = \Delta_h$, and only increase the polynomial order from p to $p + k$ with $k = 1, 2$, and 3, respectively. It can be seen that $\kappa^{\mathrm{FD}}_{S^{p+k}_{\Delta_h}}$ has the performance similar to its exact version κ^{FD} and it converges to κ^{FD}, even for $k = 1$.

Figure 5 graphs the exact temporal error ratio β and its estimate β^{FD}. In the case of linear element $p = 1$, for which the spatial error is significant, we can see that β^{FD} is a good approximation of β. Again we can see that as the temporal error becomes dominant, β^{FD} converges to β such as the case of $p = 3$. We can also observe that β is bounded by β^{FD} for this example. Note that β^{FD} is not computable, since it employs the exact solution $\widehat{U}$ of the elliptic reconstruction problem.

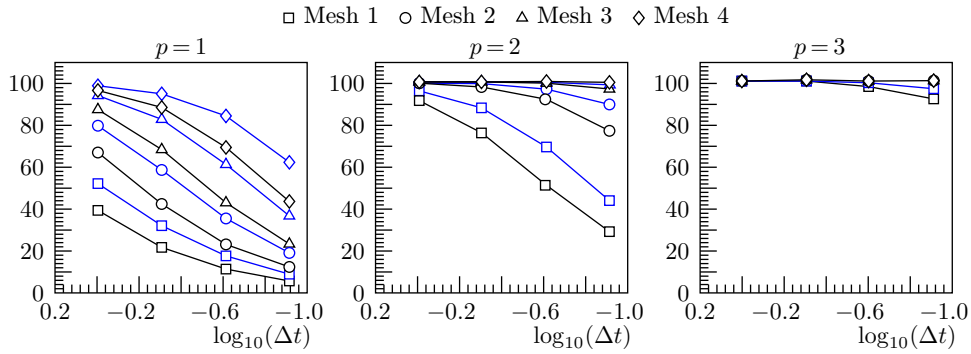


Figure 5. Heat transfer problem in one dimension. The exact temporal error ratio β (black line) and the estimated temporal error ratio β^{FD} (blue line) for the fully discrete finite element solutions of degree $p = 1, 2$, and 3 computed with four different mesh sizes and four different time step sizes.

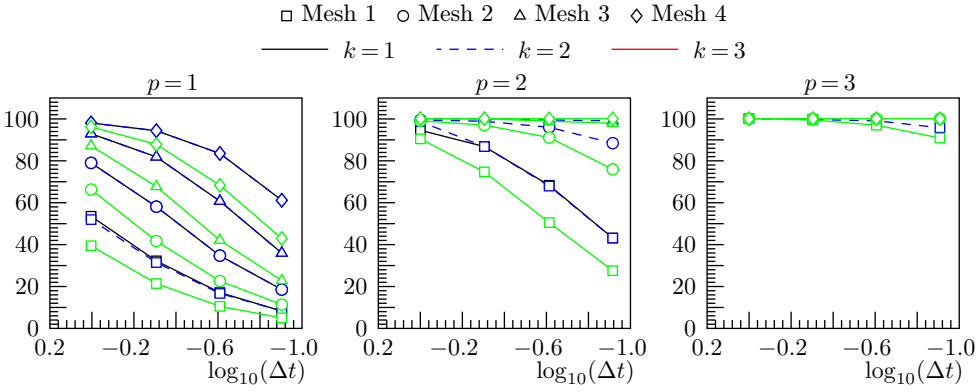


Figure 6. Heat transfer problem in one dimension. The exact temporal error ratio β (black line) and the estimated temporal error ratio $\beta^{\mathrm{FD}}_{S^{p+k}_{\Delta_{h'}}}$ (blue line) for the fully discrete finite element solutions of degree $p = 1, 2$, and 3 computed with four different mesh sizes and four different time step sizes.

Figure 6 compares the exact temporal error ratio β and its approximation $\beta^{\mathrm{FD}}_{S^{p+k}_{\Delta_{h'}}}$. It can be seen that $\beta^{\mathrm{FD}}_{S^{p+k}_{\Delta_{h'}}}$ converges to its exact version β^{FD} as shown in Figure 5 even with $k = 1$. Note that $\beta^{\mathrm{FD}}_{S^{p+k}_{\Delta_{h'}}}$ is computable since it is based on $\widehat{U}_{S^{p+k}_{\Delta'}}$.

E x a m p l e 4.2. Two dimensional synthetic problem. We consider the problem

$$\frac{\partial u}{\partial t} - \frac{\partial^2 u}{\partial x^2} - \frac{\partial^2 u}{\partial y^2} = f \quad \text{on } \Omega_T = \Omega \times (0, T], \tag{4.3a}$$

$$u = 0 \quad \text{on } \partial\Omega, \tag{4.3b}$$

$$u(x, y, 0) = 100\mathrm{e}^{-800(x-x_m)^2(y-y_m)^2} \sin(\pi x) \sin^2(\pi y) \tag{4.3c}$$

with exact solution

$$u_{EX}(x, y, t) = 100\mathrm{e}^{-10t-800(x-x_m)^2(y-y_m)^2} \sin(\pi x) \sin^2(\pi y) \tag{4.3d}$$

and $\Omega \stackrel{\text{def}}{=} (0, L) \times (0, L)$, $L = 1$, $T = 0.2$, and $x_m = y_m = 0.1$.

Figure 7 graphs the relative error ε for the fully discrete finite element solution $U_{S^p_{\Delta_h}}$. It can be seen that the relative error is not sensitive to the time step size which means that the spatial error is dominant as seen in Figure 8, which graphs the ratio of the spatial error to the total error α and the ratio of the temporal error to the total error β. Note that for coarse mesh, such as Mesh 1, the relative error can be close to 100% for element of degree $p = 1$ and 2.

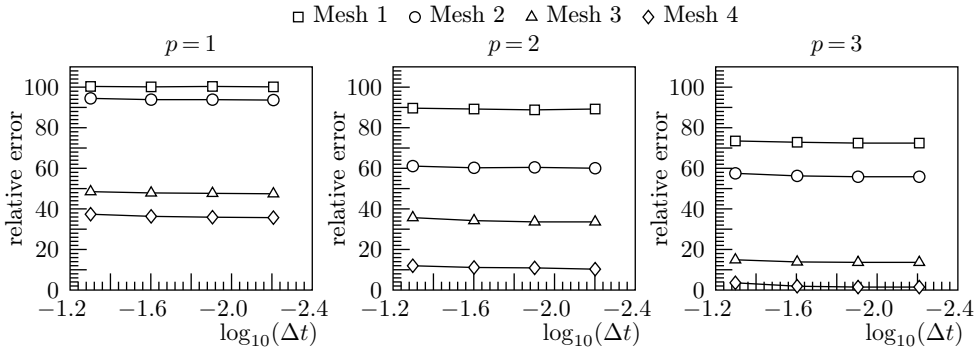


Figure 7. Two dimensional synthetic problem. The relative error ε for the fully discrete finite element solutions of degree $p = 1, 2$, and 3 computed with four different mesh sizes and four different time step sizes.

Figure 9 graphs the effectivity index κ^{FD} for the total error $\|E_h\|_{\mathscr{E}}$ and the effectivity index $\zeta^{\mathrm{FD}}_{S^p_{\Delta_h}}$ for the temporal error $\|\theta_h\|_{\mathscr{E}}$ for the fully discrete finite element solutions $U_{S^p_{\Delta_h}}$. It can be seen that κ^{FD} is close to 1 and not sensitive to the time step size due to the fact that spatial error is dominant. The maximum effectivity index $\zeta^{\mathrm{FD}}_{S_{\Delta_h}}$ for the temporal error $\|\theta_h\|_{\mathscr{E}}$ is less than 1.6, which happens to Mesh 1 and linear element $p = 1$.

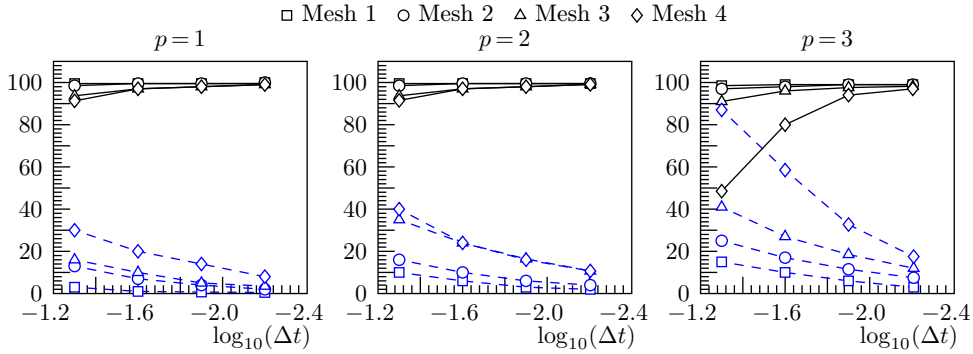


Figure 8. Two dimensional synthetic problem. The ratio of temporal error β (blue line) and the ratio of spatial error α (black line) for the fully discrete finite element solutions of degree $p = 1, 2$, and 3 computed with four different mesh sizes and four different time step sizes.

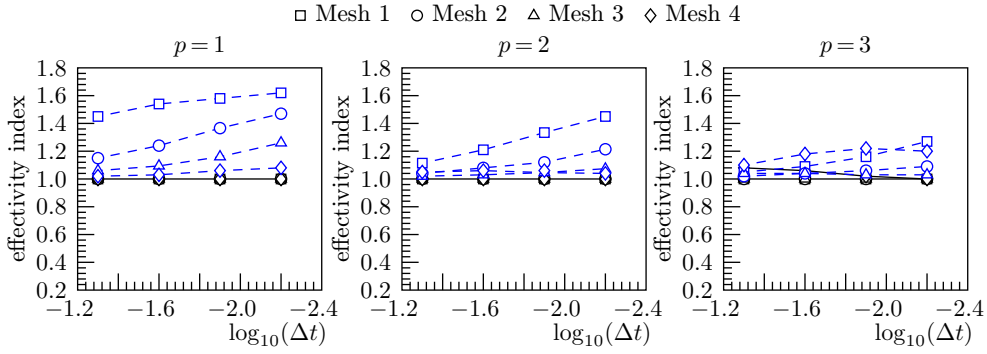


Figure 9. Two dimensional synthetic problem. The effectivity index κ^{FD} (black line) for the total error $\|E_h\|_{\mathscr{E}}$ and the effectivity index $\zeta^{\mathrm{FD}}_{S^p_{\Delta_h}}$ (blue line) for the temporal error $\|\theta_h\|_{\mathscr{E}}$ for the fully discrete finite element solutions of degree $p = 1, 2$, and 3 computed with four different mesh sizes and four different time step sizes.

Figure 10 graphs the effectivity index $\kappa^{\mathrm{FD}}_{S^p_{\Delta_{h'}}}$ based on $\widehat{U}_{S^{p+k}_{\Delta_{h'}}}$, which is the finite element approximation of the exact solution $\widehat{U}$ of degree $p + k$, computed with the mesh $\Delta_{h'}$ obtained from the uniform nested subdivision of the mesh Δ_h employed to obtain the fully discrete finite element solution $U_{s^p_{\Delta_h}}$. Here for simplicity, we fix the mesh, i.e., $\Delta_{h'} = \Delta_h$, and only increase the polynomial order from degree p to degree $p + k$ with $k = 1, 2$, and 3, respectively. It can be seen that $\kappa^{\mathrm{FD}}_{S^{p+k}_{\Delta}}$ converges to its exact version κ^{FD} with the increase of element order $p + k$. For $k = 1$, the effectivity index $\kappa^{\mathrm{FD}}_{S^p_{\Delta_{h'}}}$ can be as small as 0.4. However, with the increase of k, the effectivity index is significantly improved.

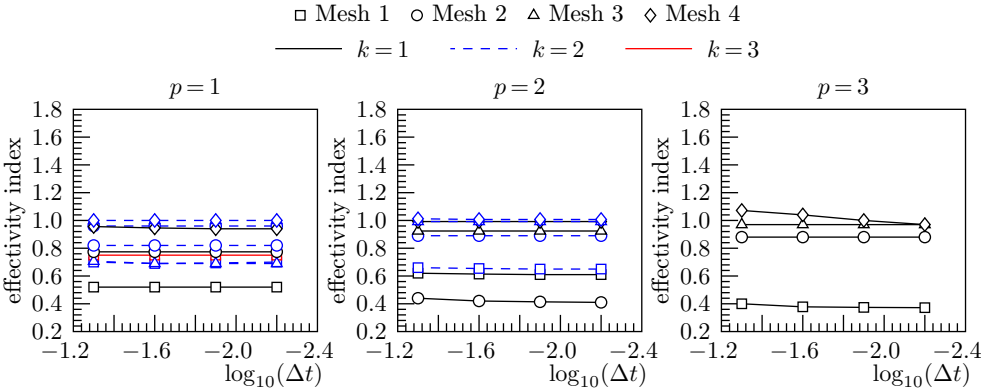


Figure 10. Two dimensional synthetic problem. The effectivity index $\kappa^{\mathrm{FD}}_{S^{p+k}_{\Delta_h}}$ for the total error $\|E_h\|_{\mathscr{E}}$ for the fully discrete finite element solutions of degree $p = 1, 2,$ and 3 computed with four different mesh sizes and four different time step sizes.

Figure 11 graphs the exact temporal error ratio β and its estimate β^{FD}. It can be seen that β^{FD} is a very good approximation of β. Again β^{FD} is not computable since it employs the exact solution $\widehat{U}$ of the elliptic reconstruction problem.

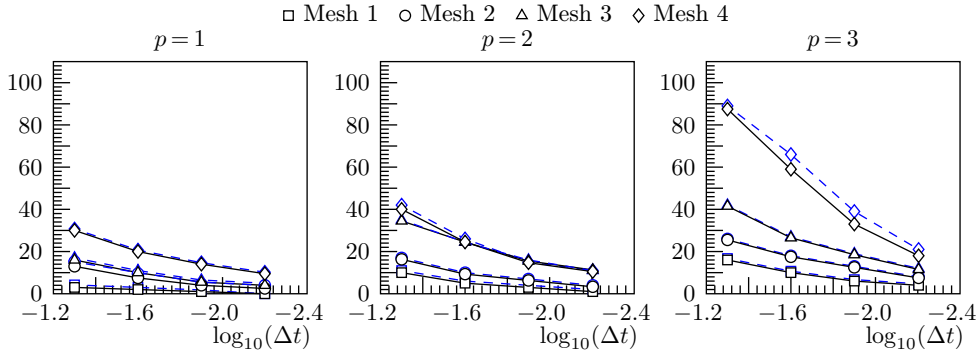


Figure 11. Two dimensional synthetic problem. The exact temporal error ratio β (black line) and the estimated temporal error ratio β^{FD} (blue line) for the fully discrete finite element solutions of degree $p = 1, 2,$ and 3 computed with four different mesh sizes and four different time step sizes.

Figure 12 compares the exact temporal error ratio β and its approximation $\beta^{\mathrm{FD}}_{S^{p+k}_{\Delta_h}}$. It can be seen that $\beta^{\mathrm{FD}}_{S^{p+k}_{\Delta_h}}$ converges to its exact version β^{FD} as shown in Figure 11 with the increase of k. Moreover, $\beta^{\mathrm{FD}}_{S^{p+k}_{\Delta_{h'}}}$ is a good approximation of β. Note that β is bounded by $\beta^{\mathrm{FD}}_{S^{p+k}_{\Delta_{h'}}}$ and $\beta^{\mathrm{FD}}_{S^{p+k}_{h'}}$ is computable since it is based on $\widehat{U}_{S^{p+k}_{\Delta_{h'}}}$.

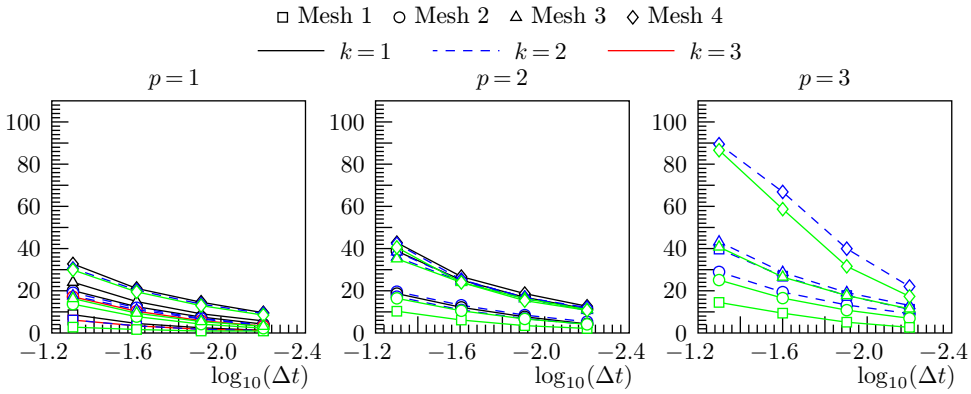


Figure 12. Two dimensional synthetic problem. The exact temporal error ratio β (black line) and the estimated temporal error ratio $\beta^{\mathrm{FD}}_{S^{p+k}_{\Delta_{h'}}}$ (blue line) for the fully discrete finite element solutions of degree $p = 1, 2$, and 3 computed with four different mesh sizes and four different time step sizes.

E x a m p l e 4.3. L-shaped domain problem. We will analyze the quality of the error estimates for the nonstationary heat-conduction problem in the L-shaped domain problem shown in Figure 13 (a):

$$\frac{\partial u}{\partial t} - \frac{\partial^2 u}{\partial x^2} - \frac{\partial^2 u}{\partial y^2} = f \quad \text{on } \Omega_T = \Omega \times (0, T], \tag{4.4a}$$

$$u = 0 \quad \text{on } \Gamma_d, \tag{4.4b}$$

$$\frac{\partial u}{\partial n} = \frac{\partial u_{EX}}{\partial n} \quad \text{on } \Gamma_N, \tag{4.4c}$$

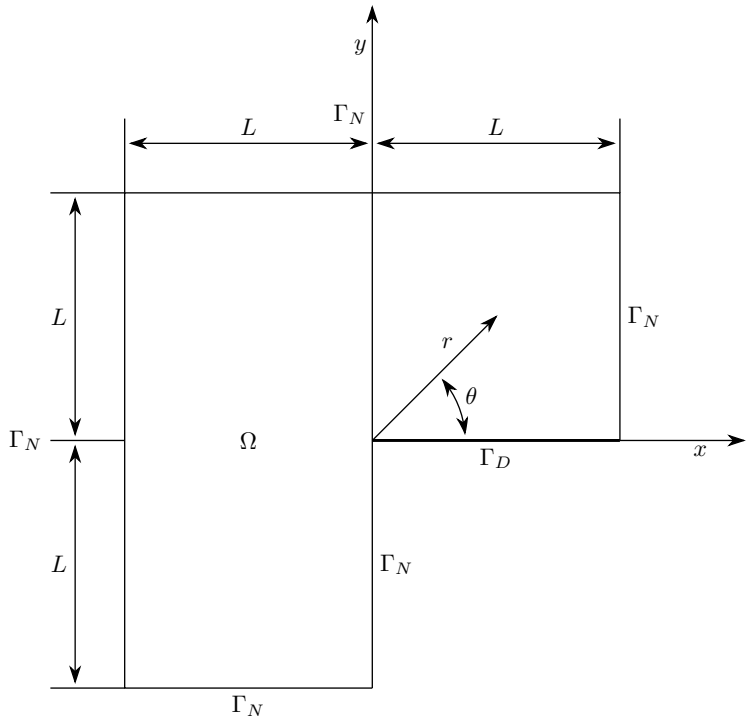
$$u(x, y, 0) = 0 \tag{4.4d}$$

with right-hand side f corresponding to the exact solution

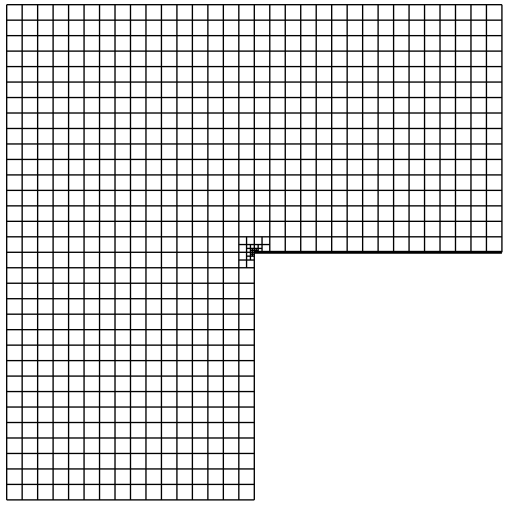
$$u_{EX}(r, \theta, t) = 10\ r^{1/3} \sin\Big(\frac{\theta}{3}\Big) \sin(3\pi t), \tag{4.4e}$$

where we have employed $T = 0.5$, $L = 1$, and $r = \sqrt{x^2 + y^2}$.

Figure 14 graphs the relative error ε versus the time-step size for the fully discrete finite element solution $U_{s^p_{\Delta_h}}$. It can be seen that the relative error is about 100% when the number of time steps N is equal to 4 and with the increase in time steps the relative error decreases dramatically. The relative error is not sensitive to the polynomial order p and the mesh refinement, which indicates that the temporal error is dominant. Figure 15 graphs the ratio of the spatial error to the total error α and the ratio of the temporal error to the total error β versus the time-step size. It can be seen that the temporal error is dominant for all the cases except the case, where $N = 4$, $p = 1$ and where Mesh 1 is employed, where the spatial error becomes dominant.



(a)



(b)

Figure 13. L-shaped domain problem. (a) The problem domain and the boundary conditions; (b) The mesh employed to obtain overkill solution.

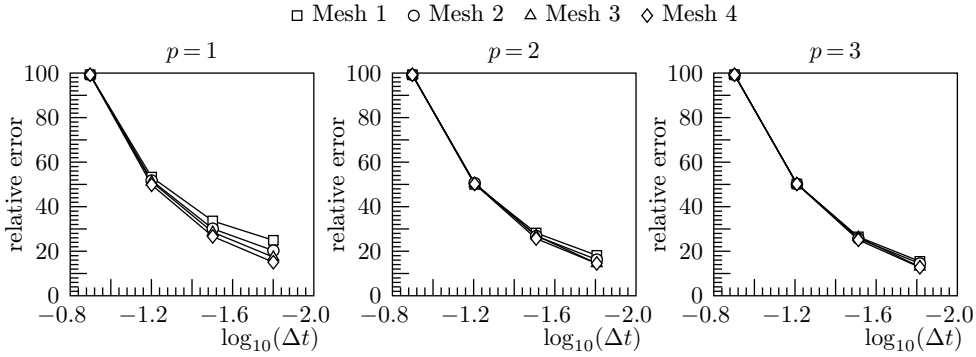


Figure 14. L-shaped domain problem. The relative error ε for the fully discrete finite element solutions of degree $p = 1, 2$, and 3 computed with four different mesh sizes and four different time step sizes.

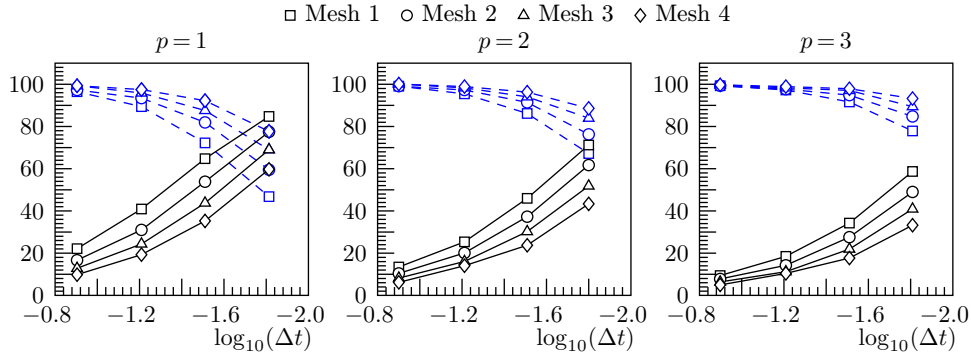


Figure 15. L-shaped domain problem. The ratio of temporal error β (blue line) and the ratio of spatial error α (black line) for the fully discrete finite element solutions of degree $p = 1, 2$, and 3 computed with four different mesh sizes and four different time step sizes.

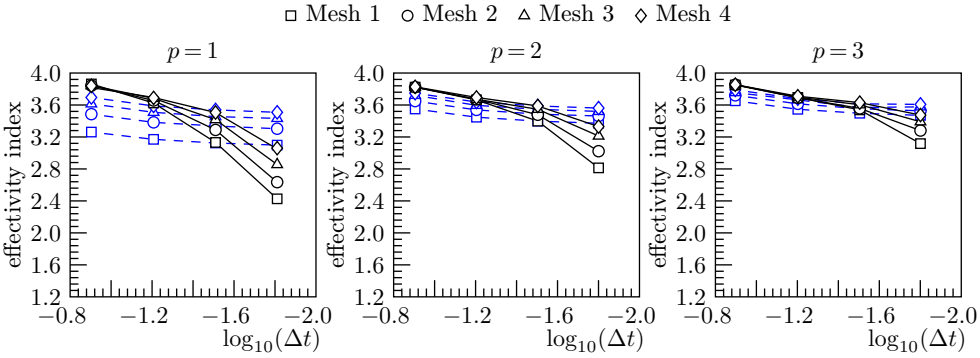


Figure 16. L-shaped domain problem. The effectivity index κ^{FD} (black line) for the total error $\|E_h\|_{\mathscr{E}}$ and the effectivity index $\zeta^{\mathrm{FD}}_{S^p_{\Delta_h}}$ (blue line) for the temporal error $\|\theta_h\|_{\mathscr{E}}$ for the fully discrete finite element solutions of degree $p = 1, 2$, and 3 computed with four different mesh sizes and four different time step sizes.

Figure 16 graphs the effectivity index κ^{FD} for the total error $\|E_h\|_{\mathscr{E}}$ and the effectivity index $\zeta^{\mathrm{FD}}_{S_{\Delta_h}}$ for the temporal error $\|\theta_h\|_{\mathscr{E}}$ for the fully discrete finite element solutions $U_{S^p_{\Delta_h}}$ versus the time-step size. It can be seen that the best number of κ^{FD} is close to 2.4, which happens to the case $N = 32$, $p = 1$ and Mesh 1. In the case when the temporal error is dominant, such as $p = 3$ as shown in Figure 8, the effectivity index $\zeta^{\mathrm{FD}}_{S_{\Delta_h}}$ for the temporal error $\|\theta_h\|_{\mathscr{E}}$ is close to κ^{FD}.

Figure 17 graphs variation, with the time-step, of the effectivity index $\kappa^{\mathrm{FD}}_{S^{p+k}_{h_h}}$ based on $\widehat{U}_{S^{p+k}_{h_h}}$, which is the finite element approximation of the exact solution $\widehat{U}$ of degree $p + k$, computed with the mesh $\Delta_{h'}$ obtained from the uniform nested subdivision of the mesh Δ_h employed to obtain the fully discrete finite element solution $U_{s^p_{\Delta_h}}$. Here for simplicity, we fix the mesh, i.e., $\Delta_{h'} = \Delta_h$, and only increase the polynomial order from degree p to degree $p + k$ with $k = 1, 2$, and 3, respectively. It can be seen that $\kappa^{\mathrm{FD}}_{S^{p+k}_{\Delta_h}}$ converges to its exact version κ^{FD} with the increase of element order $p+k$.

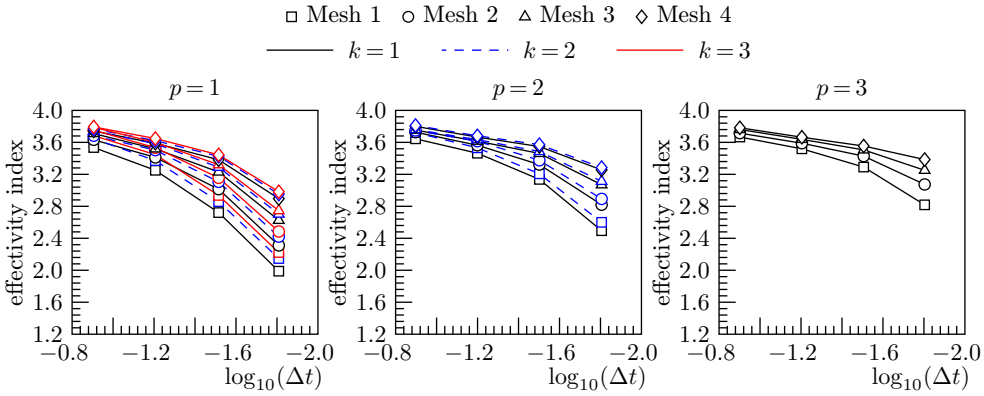


Figure 17. L-shaped domain problem. The effectivity index $\kappa^{\mathrm{FD}}_{S^{p+k}_{\Delta'}}$ for the total error $\|E_h\|_{\mathscr{E}}$ for the fully discrete finite element solutions of degree $p = 1, 2$, and 3 computed with four different mesh sizes and four different time step sizes.

Figure 18 is the illustration of the exact temporal error ratio β and its estimate β^{FD}. It can be seen that β^{FD} is a very good approximation of β. Again β^{FD} is not computable since it employs the exact solution $\widehat{U}$ of the elliptic reconstruction problem.

Figure 19 graphs the exact temporal error ratio β versus its approximation $\beta^{\mathrm{FD}}_{S_{\Delta_{h'}}}$. It can be seen that $\beta^{\mathrm{FD}}_{S^{p+k}_{\Delta_{h'}}}$ converges to its exact version β^{FD} with the increase of k. Moreover, $\beta^{\mathrm{FD}}_{S^{p+k}_{\Delta_{h'}}}$ is a good approximation of β. Note that β is bounded by $\beta^{\mathrm{FD}}_{S^{p+k}_{\Delta_{h'}}}$ and $\beta^{\mathrm{FD}}_{S^{p+k}_{\Delta^p_{h'}}}$ is computable since it is based on $\widehat{U}_{S_{\Delta^{p+k}_{h'}}}$.

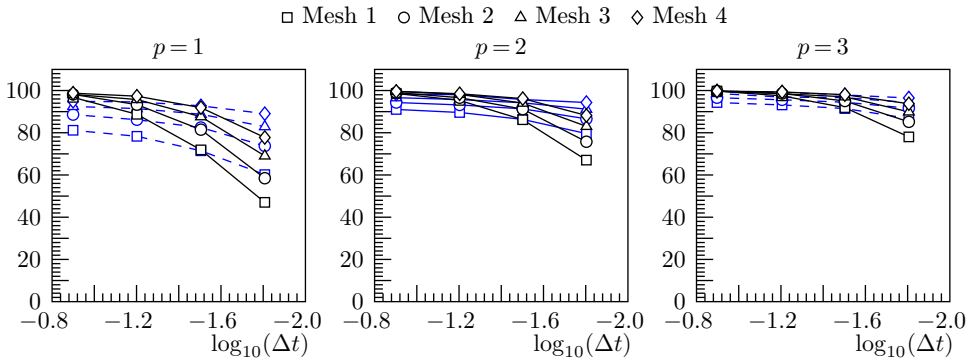


Figure 18. L-shaped domain problem. The exact temporal error ratio β (black line) and the estimated temporal error ratio β^{FD} (blue line) for the fully discrete finite element solutions of degree $p = 1, 2$, and 3 computed with four different mesh sizes and four different time step sizes.

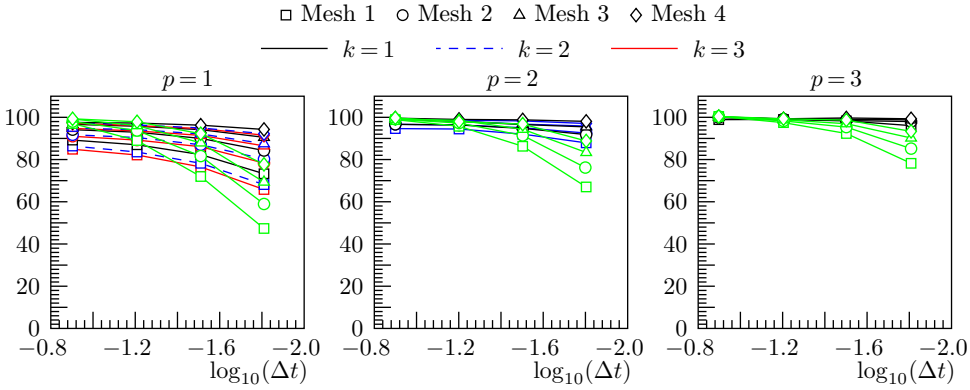


Figure 19. L-shaped domain problem. The exact temporal error ratio β (black line) and the estimated temporal error ratio $\beta^{\mathrm{FD}}_{S^{p+k}_{\Delta_{h'}}}$ (blue line) for the fully discrete finite element solutions of degree $p = 1, 2$, and 3 computed with four different mesh sizes and four different time step sizes.

E x a m p l e 4.4. Transient diffusion problem in a thermal battery. We will now analyze the quality of the estimators for a problem with several algebraic singularities at multimaterial points. The problem of the transient heat conduction in a thermal battery [4] modeled as a problem of orthotropic transient heat conduction in the multi-material domain Ω, consisting of five material subdomains Ω_k, $\overline{\Omega} = \bigcup_{k=1}^{5} \overline{\Omega}_k$, with boundary $\Gamma_N = \partial\Omega$, consisting of four parts Γ_N^i, $\overline{\Gamma}_N = \bigcup_{k=1}^{5} \overline{\Gamma}_N^i$, as shown in Figure 20, and $t \in (0, 3000)$, namely,

$$\gamma \frac{\partial u}{\partial t} - \nabla \cdot (\mathbf{K} \nabla u) = f(:, t) \stackrel{\mathrm{def}}{=} \begin{cases} 1 & \text{in } \Omega_2, \Omega_3 \\ 0 & \text{elsewhere} \end{cases} \tag{4.5a}$$

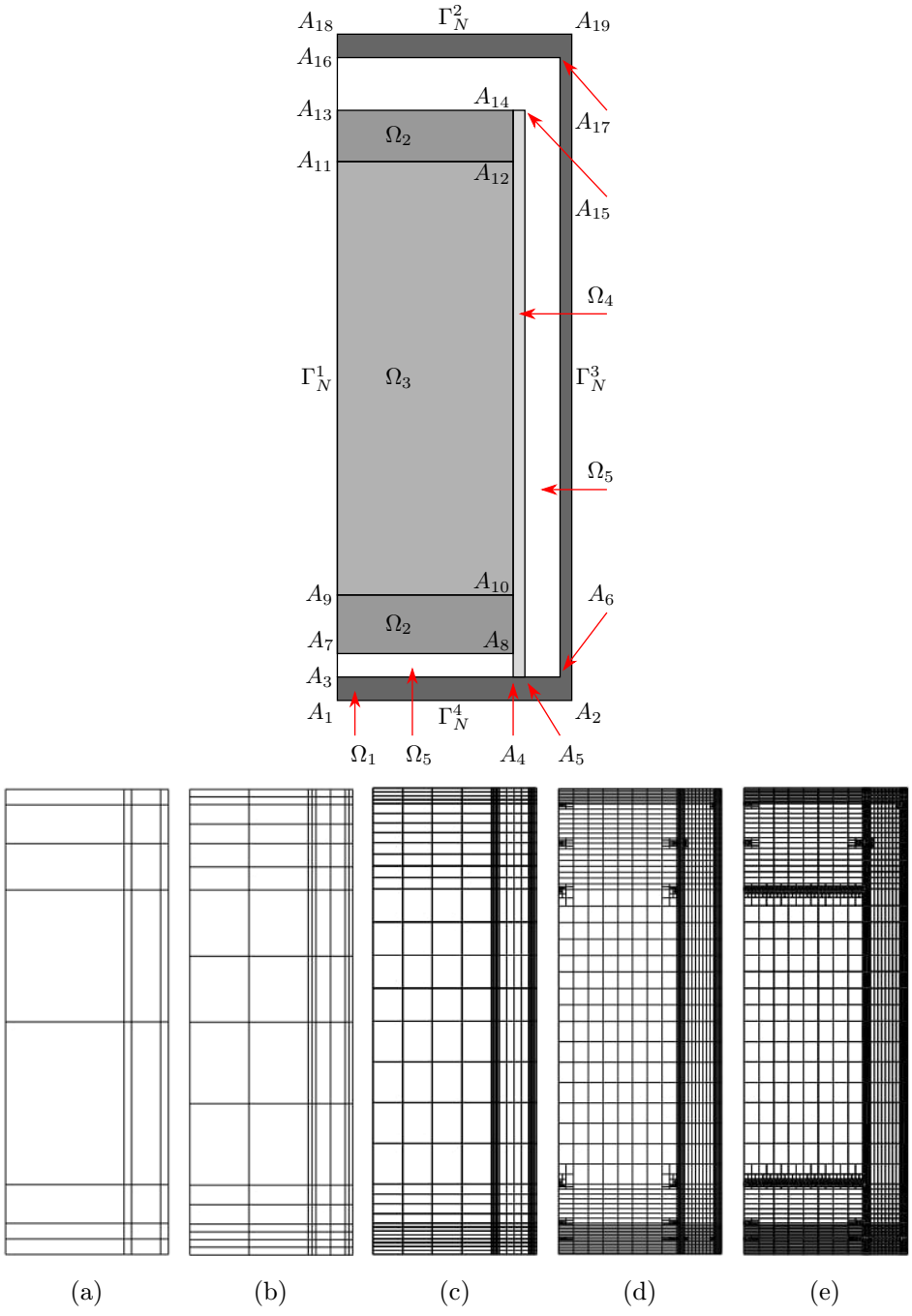


Figure 20. Transient diffusion problem in a thermal battery. The problem domain, its subdomains and the boundary with its subdomains, Meshes I, II, and III, and the overkill meshes employed.

with $\mathbf{K}$, and γ constant in each material subdomain Ω_k given below, and boundary condition

$$\mathbf{K}\nabla u \cdot \mathbf{n} = g^{(i)}(:,t) - \alpha^{(i)}(:,t)u \quad \text{on } \Gamma_N^i \tag{4.5b}$$

for $i = 1, 2, 3$, and 4, where $\alpha^{(i)}(:,t) = \alpha^{(i)}$ and $g^{(i)}(:,t) = g^{(i)}$ are defined as

$$\alpha^{(i)} = \begin{cases} 0, & i = 1 \\ 1, & i = 2 \\ 2, & i = 3 \\ 3, & i = 4 \end{cases}, \qquad g^{(i)} = \begin{cases} 0, & i = 1 \\ 3, & i = 2 \\ 2, & i = 3 \\ 1, & i = 4 \end{cases} \tag{4.5c}$$

for $0 < t \leqslant 3000$, and with the initial condition

$$u(:,0) = 0 \quad \text{in } \Omega. \tag{4.5d}$$

We will consider the orthotropic case with Ω_k, with $\mathbf{K}_{\text{Orth}}^{(k)} = \begin{bmatrix} K_x^{(k)} & 0 \\ 0 & K_y^{(k)} \end{bmatrix}$ and

$$K_x^{(k)} = \begin{cases} 25.0, & k = 1 \\ 7.0, & k = 2 \\ 5.0, & k = 3 \\ 0.2, & k = 4 \\ 0.05, & k = 5 \end{cases}, \quad K_y^{(k)} = \begin{cases} 25.0, & k = 1 \\ 0.8, & k = 2 \\ 0.0001, & k = 3 \\ 0.2, & k = 4 \\ 0.05, & k = 5 \end{cases}. \tag{4.5e}$$

We will also consider the isotropic case in which $\mathbf{K}_{\text{Iso}}^{(k)} = \begin{bmatrix} K_x^{(k)} & 0 \\ 0 & K_x^{(k)} \end{bmatrix}$ and the following γ are employed:

$$\gamma^{(k)} = \begin{cases} 4.0, & k = 1 \\ 1.8, & k = 2 \\ 3.2, & k = 3 \\ 0.1, & k = 4 \\ 0.3, & k = 5 \end{cases}. \tag{4.5f}$$

Figure 21 (or 22) is the relative error for isotropic case (or orthotropic case), where the exact solution u is approximated by the overkill solution $u_{S_{\Delta_h^{p'+k}}}$ computed with $p' = 8$ and overkill mesh as shown in Figure 20 (d) (or 20 (e)). It can be seen that for both cases the relative error becomes smaller with the increase of the number of time steps.

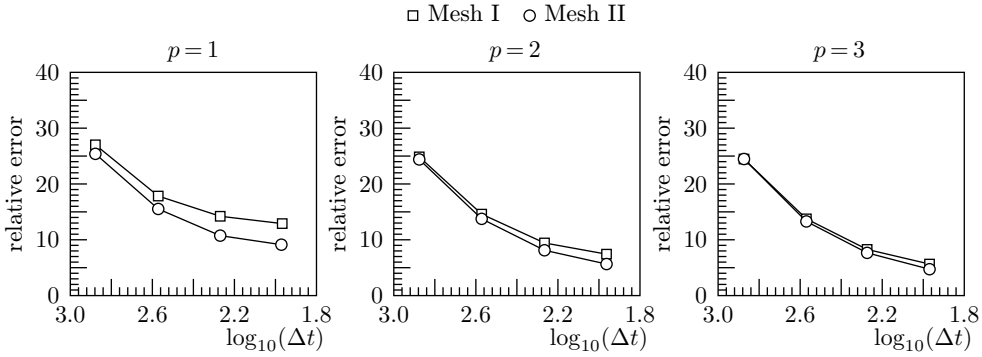


Figure 21. Transient diffusion problem in a thermal battery. The relative error ε for the fully discrete finite element solutions of degree $p = 1, 2$, and 3 computed with Mesh I and II and four different time step sizes in the isotropic case.

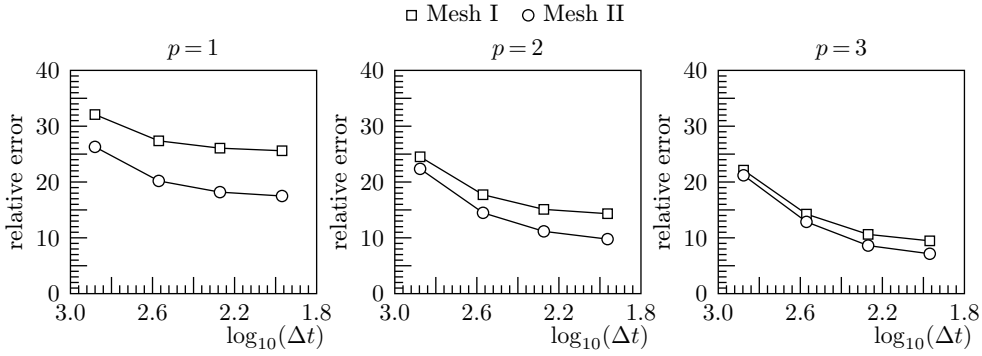


Figure 22. Transient diffusion problem in a thermal battery. The relative error ε for the fully discrete finite element solutions of degree $p = 1, 2$, and 3 computed with Mesh I and II and four different time step sizes in the orthotropic case.

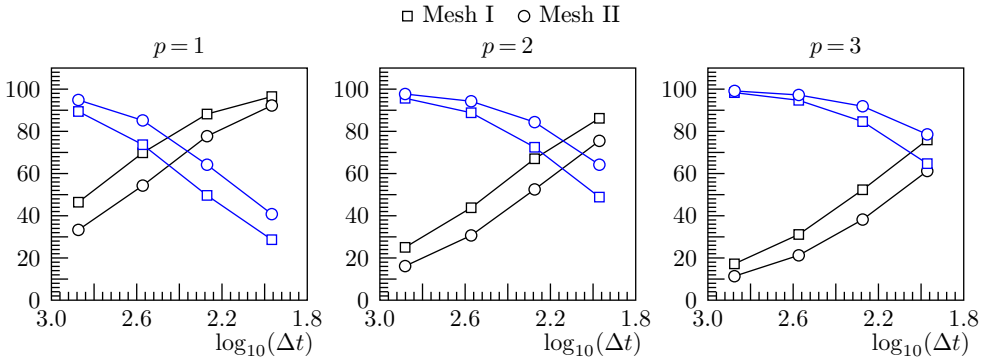


Figure 23. Transient diffusion problem in a thermal battery. The ratio of temporal error β (blue line) and the ratio of spatial error α (black line) for the fully discrete finite element solutions of degree $p = 1, 2$, and 3 computed with Mesh I and II and four different time step sizes in the isotropic case.

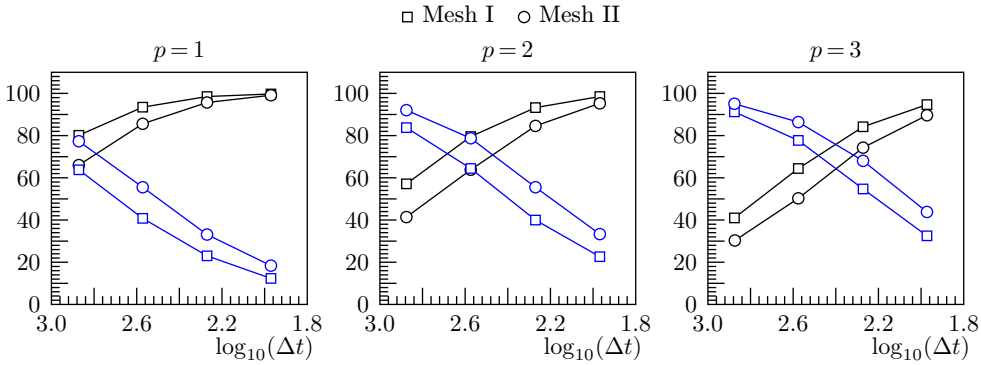


Figure 24. Transient diffusion problem in a thermal battery. The ratio of temporal error β (blue line) and the ratio of spatial error α (black line) for the fully discrete finite element solutions of degree $p = 1, 2$, and 3 computed with Mesh I and II and four different time step sizes in the orthotropic case.

Figure 23 (or 24) graphs the variation with the size of the time step, of the ratio of spatial error to the total error α and the ratio of the temporal error to the total error β for the fully discrete finite element solution $U_{s^p_{\Delta_h}}$ in the isotropic case (or orthotropic case). For isotropic case, it can be seen that the temporal error is dominant for large step size, e.g., $\Delta t = T/2^2$ and $T/2^3$. For a smaller time step size, the spatial error becomes dominant. For the orthotropic case, in the case of linear element $p = 1$, the spatial error is dominant for all the four different time step sizes. In the case of $p = 2$ and 3, the temporal error is dominant for large time step size, e.g., $\Delta t = T/2^2$, and the spatial error becomes dominant once smaller time size is chosen, e.g., $\Delta t = T/2^5$.

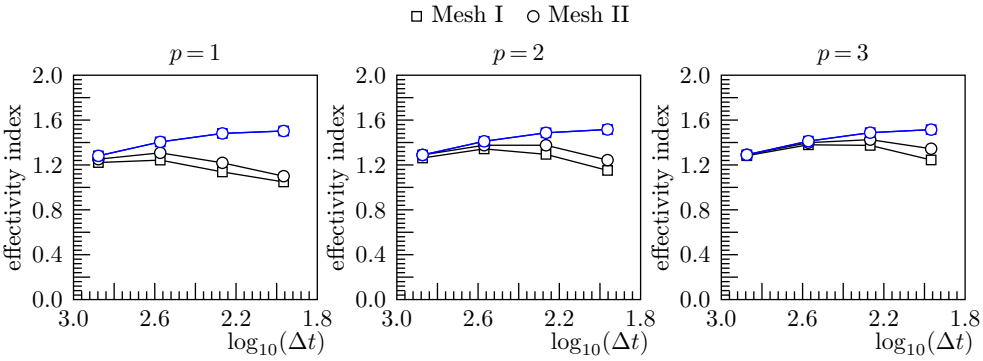


Figure 25. Transient diffusion problem in a thermal battery. The effectivity index κ^{FD} (black line) for the total error $\|E_h\|_{\mathscr{E}}$ and the effectivity index $\zeta^{\mathrm{FD}}_{S^p_{\Delta_h}}$ (blue line) for the temporal error $\|\theta_h\|_{\mathscr{E}}$ for the fully discrete finite element solutions of degree $p = 1, 2$, and 3 computed with Mesh I and II and four different time step sizes in the isotropic case.

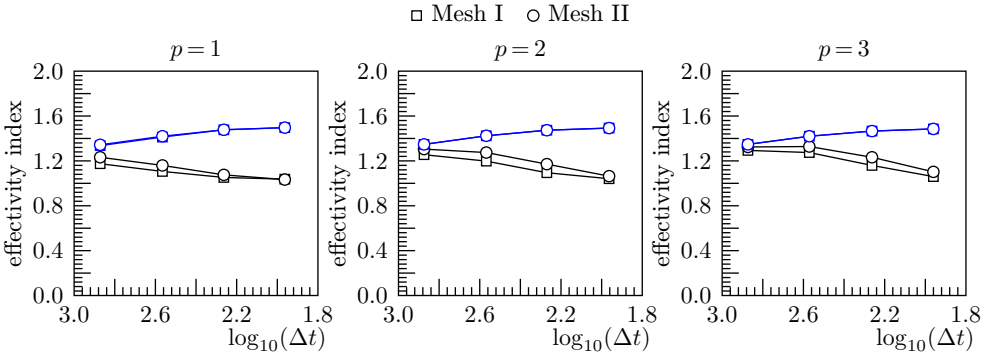


Figure 26. Transient diffusion problem in a thermal battery. The effectivity index κ^{FD} (black line) for the total error $\|E_h\|_{\mathscr{E}}$ and the effectivity index $\zeta^{\mathrm{FD}}_{S^p_{\Delta_h}}$ (blue line) for the temporal error $\|\theta_h\|_{\mathscr{E}}$ for the fully discrete finite element solutions of degree $p = 1, 2$, and 3 computed with Mesh I and II and four different time step sizes in the orthotropic case.

Figure 25 (or 26) shows the variation of the effectivity index κ^{FD} for the total error $\|E_h\|_{\mathscr{E}}$ and the effectivity index $\zeta^{\mathrm{FD}}_{S_{\Delta_h}}$ for the temporal error $\|\theta_h\|_{\mathscr{E}}$ for the fully discrete finite element solutions $U_{S^p_{\Delta_h}}$ of degree $p = 1, 2$, and 3 in the isotropic case (or orthotropic case). It can be seen that κ^{FD} is close to 1 for both isotropic case and orthotropic case, and the maximum effectivity index $\zeta^{\mathrm{FD}}_{S^p_{\Delta_h}}$ for the temporal error is less than 1.6. We can also observe that if the temporal error is dominant, κ^{FD} is close to $\zeta^{\mathrm{FD}}_{S^p_{\Delta_h}}$. For example, we can see from Figure 23 that in the isotropic case with time step size $\Delta t = T/2^2$ and $p = 2, 3$, the temporal error is dominant and about 100%. In Figure 25, we find that κ^{FD} is equal to $\zeta^{\mathrm{FD}}_{S^p_{\Delta_h}}$. This phenomenon can also be observed for orthotropic case with $p = 2$ and 3 at time step size $\Delta t = T/2^2$.

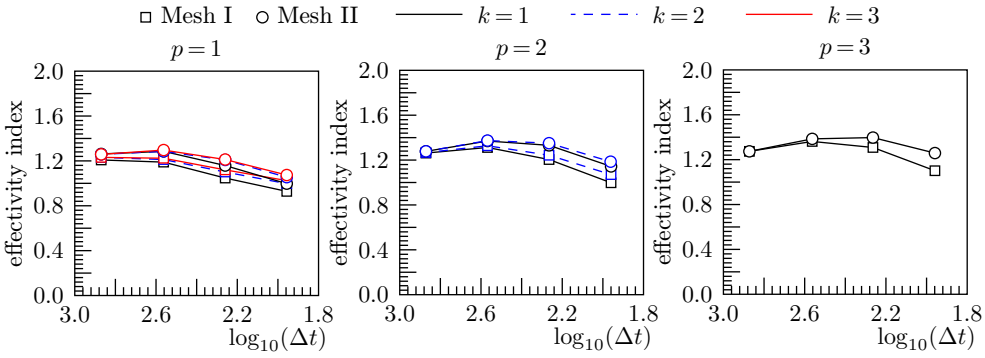


Figure 27. Transient diffusion problem in a thermal battery. The effectivity index $\kappa^{\mathrm{FD}}_{S^p_{\Delta'}}$ for the total error $\|E_h\|_{\mathscr{E}}$ for the fully discrete finite element solutions of degree $p = 1, 2$, and 3 computed with Mesh I and II and four different time step sizes in the isotropic case.

Figure 27 (or 28) graphs the effectivity index $\kappa^{\mathrm{FD}}_{S^{p+k}_{\Delta_{h'}}}$ based on $\widehat{U}_{S^{p+k}_{\Delta_{h'}}}$, which is the finite element approximation of the exact solution $\widehat{U}$ of degree $p+k$, computed with the mesh $\Delta_{h'}$ obtained from the uniform nested subdivision of the mesh Δ_h employed to obtain the fully discrete finite element solution $U_{s^p_{\Delta_h}}$. Here for simplicity, we fix the mesh, i.e., $\Delta_{h'} = \Delta_h$, and only increase the polynomial order from degree p to degree $p+k$ with $k = 1, 2$, and 3, respectively. It can be seen that $\kappa^{\mathrm{FD}}_{S^{p+k}_{\Delta_h}}$ has similar performancer as its exact version κ^{FD} and it converges to κ^{FD} even for $k = 1$.

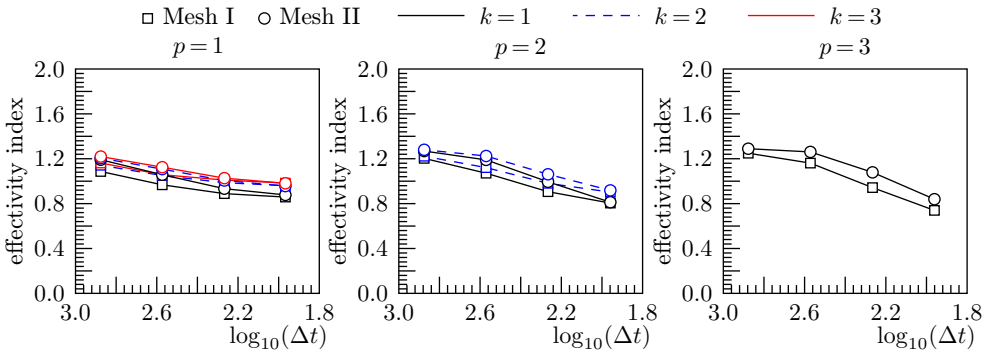


Figure 28. Transient diffusion problem in a thermal battery. The effectivity index $\kappa^{\mathrm{FD}}_{S^{p+k}_{\Delta'_h}}$ for the total error $\|E_h\|_{\mathscr{E}}$ for the fully discrete finite element solutions of degree $p = 1, 2$, and 3 computed with Mesh I and II and four different time step sizes in the orthotropic case.

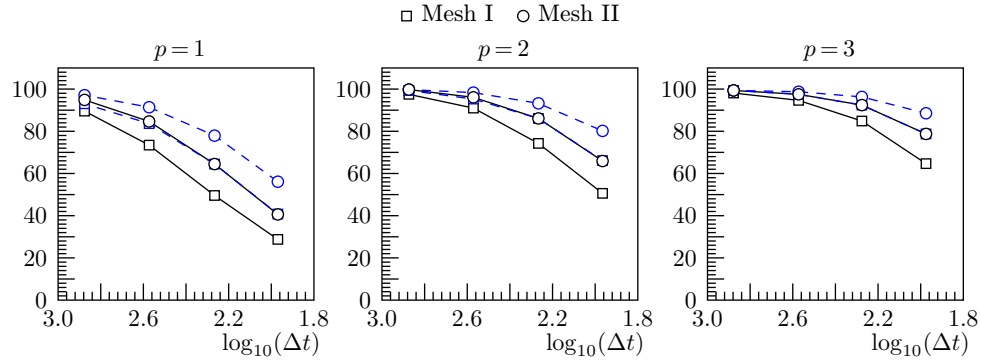


Figure 29. Transient diffusion problem in a thermal battery. The exact temporal error ratio β (black line) and the estimated temporal error ratio β^{FD} (blue line) for the fully discrete finite element solutions of degree $p = 1, 2$, and 3 computed with Mesh I and II and four different time step sizes in the isotropic case.

Figure 29 (or 30) graphs the exact temporal error ratio β and its estimate β^{FD} for isotropic case (or orthotropic case). It can be seen that β is bounded by β^{FD}. For both cases, β^{FD} is a good estimate of β. If the temporal error is dominant, we can

see that β^{FD} is very close to β. For instance, in the isotropic case with time step size $\Delta t = T/2^2$ and $p = 2, 3$, where the temporal error ratio is about 100%.

Figure 31 (or 32) compares the exact temporal error ratio β and its approximation $\beta^{\mathrm{FD}}_{S^{p+k}_{\Delta'}}$. It can be seen that $\beta^{\mathrm{FD}}_{S^{p+k}_{\Delta_{h'}}}$ converges to its exact version β^{FD} as shown in Figure 5 even with $k = 1$. Note that $\beta^{\mathrm{FD}}_{S^{p+k}_{\Delta_{h'}}}$ is computable since it is based on $\widehat{U}_{S^{p+k}_{\Delta_{h'}}}$.

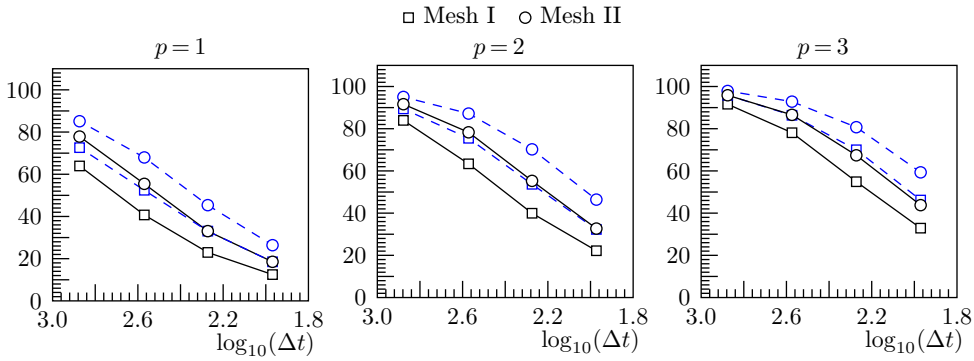


Figure 30. Transient diffusion problem in a thermal battery. The exact temporal error ratio β (black line) and the estimated temporal error ratio β^{FD} (dashed evenly line) for the fully discrete finite element solutions of degree $p = 1, 2$, and 3 computed with Mesh I and II and four different time step sizes in the orthotropic case.

5. Conclusions

In this paper we extended the elliptic reconstruction approach to construct guaranteed error estimates for fully discrete finite element solutions of the linear parabolic problem. The backward difference method was employed for time-integration, nevertheless the employed reconstruction approach can be combined with any stable time-stepping scheme. The reliability of the estimator is maintained by controlling the time-error to a small percentage of the constructed space-time error-bound. The main conclusions are:

1. The exact error in the fully discrete finite element solution $u - U_{S^p_{\Delta_h}}$ can be approximated well by $\widehat{U} - U_{S^p_{\Delta_h}}$ at time instant $t = t_n$ for each time interval $(t_{n-1}, t_n]$ only under the condition that the temporal error is negligible in comparison to the spatial error.

2. We constructed a guaranteed estimator for estimating the error in a space-time norm, the $\mathscr{C}$-norm.

3. By employing a representative set of benchmarks, we demonstrated that the proposed estimator has good effectivity, of the order of 1.6, even when the solution has

many singularities. The necessary condition that the time error must be controlled to a small percentage of the error-bound.

4. To make the control of the time-error possible, we constructed a guaranteed estimator for the contribution of the time-error to the upper bound. The time-error estimator is guaranteed upper, it has good effectivity, and hence it can be used to control the time-error to a small percentage of the space-error.

5. The control of the time-error is always possible by employing adaptive time stepping, or by increasing the order of time-approximation by using the p-version in the time domain.

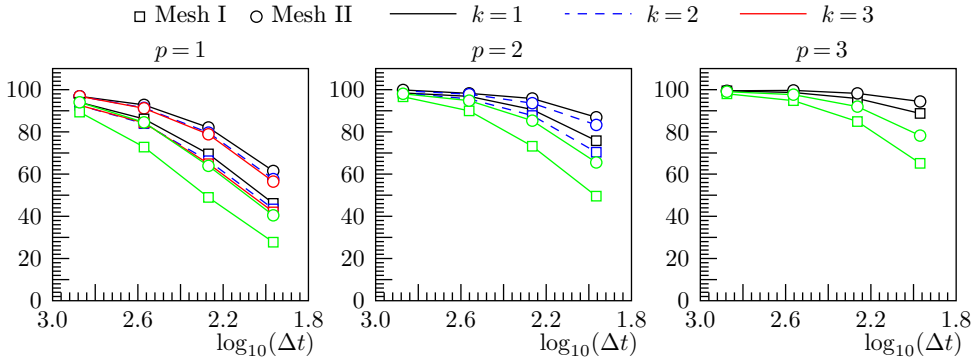


Figure 31. Transient diffusion problem in a thermal battery. The exact temporal error ratio β (black line) and the estimated temporal error ratio $\beta^{\mathrm{FD}}_{S^p_{\Delta_{h'}}}$ (blue line) for the fully discrete finite element solutions of degree $p = 1, 2$, and 3 computed with Mesh I and II and four different time step sizes in the isotropic case.

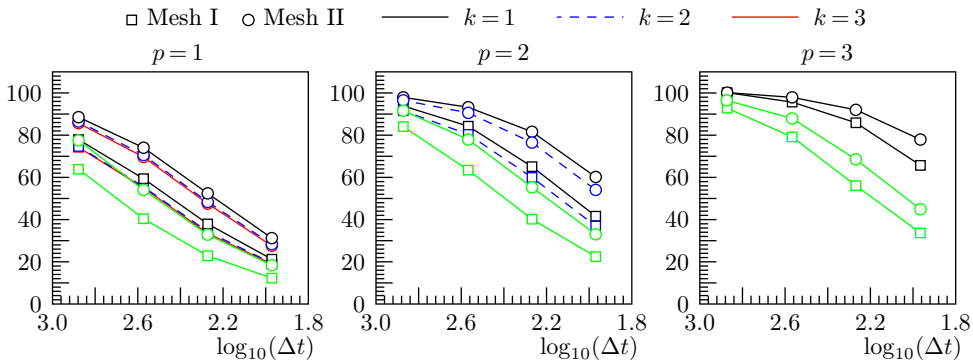


Figure 32. Transient diffusion problem in a thermal battery. The exact temporal error ratio β (black line) and the estimated temporal error ratio $\beta^{\mathrm{FD}}_{S_{\Delta'}}$ (red line) for the fully discrete finite element solutions of degree $p = 1, 2$, and 3 computed with Mesh I and II and four different time step sizes in the orthotropic case.

A c k n o w l e d g e m e n t s. This is joint work with Professor Ivo Babuška. Theofanis Strouboulis is eternally grateful to Professor Babuška for all that he had learned from him during the 30 years (1991–2021) of interactions, discussions, and collaboration. All correspondence should be addressed to Theofanis Strouboulis.

References

[1] *J. de Frutos, B. García-Archilla, J. Novo*: A posteriori error estimates for fully discrete nonlinear parabolic problems. Comput. Methods Appl. Mech. Eng. *196* (2007), 3462–3474. zbl MR doi

[2] *J. de Frutos, J. Novo*: Postprocessing the linear finite element method. SIAM J. Numer. Anal. *40* (2002), 805–819. zbl MR doi

[3] *B. García-Archilla, E. S. Titi*: Postprocessing the Galerkin method: The finite-element case. SIAM J. Numer. Anal. *37* (2000), 470–499. zbl MR doi

[4] *R. R. Lober*: Thermal Battery Life Test Problem for Residual Method Error Measure Development. Technical Report. Sandia National Laboratories, Albuquerque, New Mexico, 1999.

[5] *C. Makridakis, R. H. Nochetto*: Elliptic reconstruction and a posteriori error estimates for parabolic problems. SIAM J. Numer. Anal. *41* (2003), 1585–1594. zbl MR doi

[6] *T. Strouboulis, D. Wang, I. Babuška*: Superconvergence of elliptic reconstructions of finite element solutions of parabolic problems in domains with piecewise smooth boundaries. Comput. Methods Appl. Mech. Eng. *241-244* (2012), 128–141. zbl MR doi

[7] *V. Thomée*: Galerkin Finite Element Methods for Parabolic Problems. Springer Series in Computational Mathematics 25. Springer, New York, 1997. zbl MR doi

[8] *D. Wang*: Guaranteed Verification of Finite Element Solutions of Heat Conduction: Ph.D. Dissertation. Texas A&M University, College Station, 2012.

Authors' address: *Theofanis Strouboulis* (corresponding author), *Delin Wang*, Department of Aerospace Engineering, Texas A&M University, 400 Bizzell St., College Station, TX 77843, USA, e-mail: `strouboulis@tamu.edu`, `delinwang@gmail.com`.